J Therm Anal Calorim (2016) 124:21–33
DOI 10.1007/s10973-015-4979-0

Non-isothermal crystallization kinetics of $Zr_{52}Cu_{18}Ni_{14}Al_{10}Ti_6$ metallic glass

Sonal R. Prajapati[1] · Supriya Kasyap[1] · Ashmi T. Patel[2] · Arun Pratap[1]

Received: 5 March 2015 / Accepted: 8 August 2015 / Published online: 23 August 2015

Abstract In the present work, the thermal analysis of the bulk metallic glass with composition $Zr_{52}Cu_{18}Ni_{14}Al_{10}Ti_6$ has been done by differential scanning calorimetry (DSC) through non-isothermal method. DSC curves indicate a two-step crystallization process at all four heating rates, i.e., 5, 10, 15, and 20 °C min^{-1}. Non-isothermal crystallization studies of the alloy indicate that kinetics conform to Johnson–Mehl–Avrami (JMA) model. The master plot method and normalized heat flow curve prove the validity of JMA model. Analysis of the second crystallization event has been done by using various isoconversional and isokinetic methods available in the literature. Activation energy of crystallization increases, whereas the value of Avrami exponent decreases, with increase in crystallized fraction. The fitting curve using Lasocka's empirical relation shows that the influence of the heating rate for secondary crystallization event is larger than the primary crystallization event.

Keywords Crystallization kinetics · DSC · Secondary crystallization · Isoconversional methods · Isokinetic methods

The present article is based on the lecture presented at SATAC2014 conference in Dhanbad - India on 15–17 December, 2014.

✉ Sonal R. Prajapati
sonal051987@yahoo.in

Arun Pratap
apratapmsu@yahoo.com

[1] Condensed Matter Physics Laboratory, Applied Physics Department, Faculty of Technology and Engineering, The M. S. University of Baroda, Vadodara 390001, India

[2] Physics Department, Institute of Technology and Management Universe, Dhanora Tank Road, Paldi Village, Waghodia Taluka, Vadodara 391510, India

Introduction

Bulk metallic glasses having exceptional glass-forming ability (GFA) provide an opportunity to study the crystallization kinetics in the entire undercooled region. Crystallization process can be investigated under isothermal and non-isothermal conditions. Non-isothermal experiments can be performed more easily and faster than isothermal experiments. Moreover, they provide smaller signal-to-noise ratio for kinetic experiments [1]. So to study crystallization process under non-isothermal condition, various approximation and theoretical models have been proposed [2–6].

Crystallization kinetics of the Zr-based metallic glasses can be understood by two methods namely isokinetic and isoconversional methods. Isokinetic methods are also known as model-dependent methods since they depend upon different reaction models, and transformation mechanism remains constant with time and temperature. In case of isoconversional methods, which are known as model-free method, transformation mechanism varies with degree of conversion. Different kinetic parameters can be evaluated by both methods.

Since the discovery of Zr-based metallic glasses, various efforts have been made to understand their GFA and thermal stability against crystallization. Many studies regarding the crystallization kinetics under isothermal and non-isothermal conditions for Zr-based metallic alloys are available in the literature [7–13]. Qiao and Pelletier [14] have studied crystallization kinetics of $Zr_{55}Cu_{30}Ni_5Al_{10}$ metallic glass by isochronal and isothermal routes. Prashanth et al. [15] investigated the kinetics of $Zr_{65}Ag_{5}Cu_{12.5}Ni_{10}Al_{7.5}$ and showed that crystallization process is diffusion-controlled with three-dimensional growth. Lu et al. [16] studied the crystallization process of three

clearly separated crystallization peaks of $(Zr_{46}Cu_{42}Al_{7}Y_{5})_{95}Be_5$ by isoconversional, isokinetic, and master plots methods. More recently, Kasyap et al. [17] have carried out crystallization kinetics of $Ti_{20}Cu_{60}Zr_{20}$ metallic glass using isoconversional methods by modulated differential scanning calorimetry (DSC).

The aim of this paper was to study the second crystallization event of Zr-based metallic glass and to obtain accurate values for the activation energies of crystallization as well as other kinetic parameters. It is important to study variation in activation energy, E, with degree of crystallization as it provides useful information about the different mechanisms involved in the transformation process.

Experimental

Ingots of alloys of nominal composition $Zr_{52}Cu_{18}Ni_{14}Al_{10}Ti_6$ were obtained using arc melting technique. The amorphous ribbons of $Zr_{52}Cu_{18}Ni_{14}Al_{10}Ti_6$ composition were prepared by a single roller melt-spinning technique in an argon atmosphere at Bhabha Atomic Research Centre (BARC), Mumbai (India). EDAX was done to confirm its elemental composition of the present metallic glass. Thermal analysis of sample was carried out in a DSC-50 Shimadzu, Japan, at four different heating rates 5, 10, 15, and 20 °C min^{-1}. Aluminum pans were used as sample holders. The sample was heated in air atmosphere up to 560 °C at different heating rates.

Theoretical background

For non-isothermal crystallization kinetics, the reaction rate can be expressed by the following kinetic equation [18]:

$$\frac{d\alpha}{dT} = \frac{1}{\beta}k(T)f(\alpha) = \frac{k_0}{\beta}\exp\left(-\frac{E}{RT}\right)f(\alpha) \quad (1)$$

where $k(T)$ is the rate constant, β is the heating rate, α is the degree of conversion, and $f(\alpha)$ is the reaction model. The determination of kinetic parameters k_0, E, and $f(\alpha)$ is the chief aim of studying kinetics of crystallization. So to determine kinetic triplet, various isoconversional and isokinetic methods are used.

Isoconversional methods

Isoconversional methods are independent of reaction model $f(\alpha)$, and hence, they are also known as model-free methods. Further, model-free methods are classified as linear integral and linear differential methods. Integral isoconversional methods depend on the approximation of the temperature integral. Differential isoconversional methods are based on the rate of transformation.

Separation of variables and integration of Eq. (1) gives:

$$g(\alpha) = \int_0^{\alpha}[f(\alpha)]^{-1} = \frac{k_0}{\beta}\int_0^{T}\exp\left(-\frac{E}{RT}\right)dT \quad (2)$$

Above integral equation does not have an exact analytical solution; hence, various approximations of this integral are suggested in the literature [19–23] for the evaluation of activation energies dependent on the degree of conversion, α. Starink [21] has analyzed and discussed various isoconversional methods in terms of their applicability and limitations.

The general form of the linear equation expressing the linear integral isoconversional methods is [24]:

$$\ln\left(\frac{\beta}{T_{\alpha}^{k}}\right) = -A\frac{E_{\alpha}}{RT_{\alpha}} + C \quad (3)$$

where the parameters k and A are dependent on approximations of temperature integral, C is constant, and the subscript α designates the degree of conversion for Ozawa–Flynn–Wall (OFW) ($k = 0$, $A = 1.0516$), Kissinger–Akahira–Sunose (KAS) ($k = 2$, $A = 1$), and so on.

Isokinetic methods

These methods are model-fitting methods that depend upon the consideration of various kinds of models for the determination of kinetic parameters E and k_0. Isokinetic methods are, in general, employed to study the kinetics of phase transformations occurring in isothermal conditions. The isokinetic methods are mainly based on the Kolmogorov–Johnson–Mehl–Avrami (KJMA) rate equation [25–29], given by

$$\frac{d\alpha}{dt} = nk(1-\alpha)[-\ln(1-\alpha)]^{(n-1)/n} \quad (4)$$

where α is the degree of conversion at a particular time, n is the Avrami (growth) exponent, and $k(T)$ is the rate constant given by

$$k(T) = k_0\exp\left(-\frac{E}{RT}\right) \quad (5)$$

where k_0 is the pre-exponential factor, E is the activation energy, and R is the universal gas constant.

From Eqs. (4) and (5), transformed fraction can be expressed as

$$\alpha = 1 - \exp\left[-\frac{k_0}{\beta}\int_{T_0}^{T}\exp\left(-\frac{E}{RT}\right)dT\right]^n \quad (6)$$

The integral in Eq. (6) does not have an exact solution, and hence, one has to switch to approximations. Various

approximations have been used in the literature to obtain an accurate solution of the integral [30–32]. On employing Gorbachev approximation [32], i.e., Eq. (7), in Eq. (6), we obtain Eq. (8).

$$\int_0^T e^{-E/RT} dT = \frac{RT^2}{E + 2RT} e^{-E/RT} \tag{7}$$

$$\alpha = 1 - \exp\left[-\left\{\frac{k_0 RT^2}{\beta(E + 2RT)} \exp\left(-\frac{E}{RT}\right) dT\right\}^n\right] \tag{8}$$

The values of E, n, and k_0 can be determined by fitting the experimental data of α to Eq. (8) with the help of least square method.

Results and discussion

In order to confirm the elemental composition of $Zr_{52}Cu_{18}Ni_{14}Al_{10}Ti_6$ amorphous ribbons, energy-dispersive X-ray analysis (EDX) was performed. EDX scan of whole surface of the specimen gives an average composition of this alloy as shown in inset of Fig. 1. This value is close to the nominal composition $Zr_{52}Cu_{18}Ni_{14}Al_{10}Ti_6$.

Figure 2 shows the DSC curves for $Zr_{52}Cu_{18}Ni_{14}Al_{10}Ti_6$ at four different heating rates (5, 10, 15, and 20 °C min^{-1}). It can be observed that crystallization occurs in two steps. The first and second peaks of crystallization correspond to low temperature and high temperature, respectively. As heating rate increases, the peak shifts toward higher temperature, which implies that crystallization depends upon the heating rate during the continuous heating process. The second crystallization event is more sensitive toward heating rate as compared to first peak. Earlier, Patel et al. [33] have carried out the analysis of crystallization kinetics of $Zr_{52}Cu_{18}Ni_{14}Al_{10}Ti_6$ for the first peak by isokinetic and isoconversional methods. The analysis of the first peak

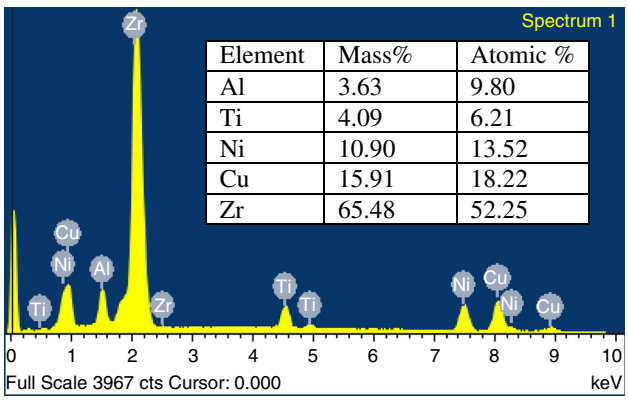

Fig. 1 Energy-dispersive X-ray analysis (EDX) of $Zr_{52}Cu_{18}Ni_{14}Al_{10}Ti_6$ amorphous ribbons

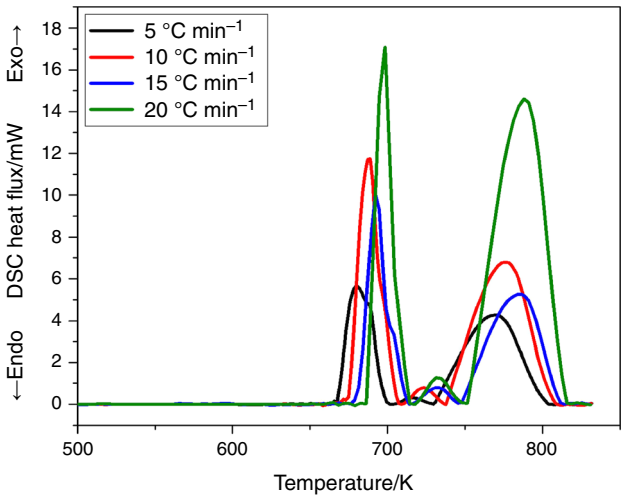

Fig. 2 DSC curve for $Zr_{52}Cu_{18}Ni_{14}Al_{10}Ti_6$

revealed that the activation energy (E) initially increases slowly in the range α (=0.3–0.6) followed by a quick increase in E with α. This indicates that second crystallization step starts even before the first step is completed. This inspires us for the analysis of next crystallization event. Also in order to understand the overall crystallization process, analysis of second peak is important. The second peak or crystallization event may have originated due to following reasons: (a) The nature of crystal produced during first crystallization is metastable. With increase in temperature, these metastable materials transform into another structure. (b) A multicomponent metallic glass does not crystallize in a single step. The crystal which persists within the melt is of different composition which crystallizes with a much slower kinetics to another phase at high temperature. (c) Some of the crystals formed during first crystallization are small, and they grow to form larger grains. The calorimetric data of this glass cannot determine which of these occurrences are more favorable [34]. A sharp peak is observed for first crystallization event due to the formation of nuclei at higher rate, whereas for the second peak, it is found to be broad as growth takes place slowly. Also, a small peak is observed around 730 K, at all heating rates. The intensity of this peak is very small as compared to the other two peaks. This less prominent peak may have occurred due to the overlapping of first and second peaks. This does not indicate any significant process. Hence, we have analyzed only the prominent peaks. The crystallized fraction, α, is calculated from DSC curve at different temperatures. The so-obtained DSC data can be analyzed by both methods, i.e., isokinetic and isoconversional.

Now to understand which method is more appropriate to study the second step crystallization process, various testing techniques are carried out to fit experimental data.

Firstly to check the validation of JMA model, experimental data of fractional crystallization are fitted by iterative least square fitting method using Eq. (8). Initial estimate of E and k_0 is calculated from Kissinger equation.

The sigmoidal shape (Fig. 3) of crystallized fraction with temperature represents the bulk crystallization and excludes the chance of surface crystallization [35]. The above sigmoidal curve represents three different stages of crystallization. In the initial stage, only nucleation occurs, and with further increase in reaction rates, both nucleation and growth of nuclei take place. Finally, due to decrease in surface area, nuclei start coalescing and hence reaction rate decreases. The perfect fitting of experimental data to Eq. (8) confirms the validity of JMA model. Table 1 reports the value of n, k_0, and E at different heating rates calculated by least square fitting method.

Malek [36] gave another testing technique for checking the validity of KJMA model in non-isothermal conditions in which two functions $y(\alpha)$ and $z(\alpha)$ are calculated. The dependence of $y(\alpha)$ and $z(\alpha)$ on α can be expressed as below:

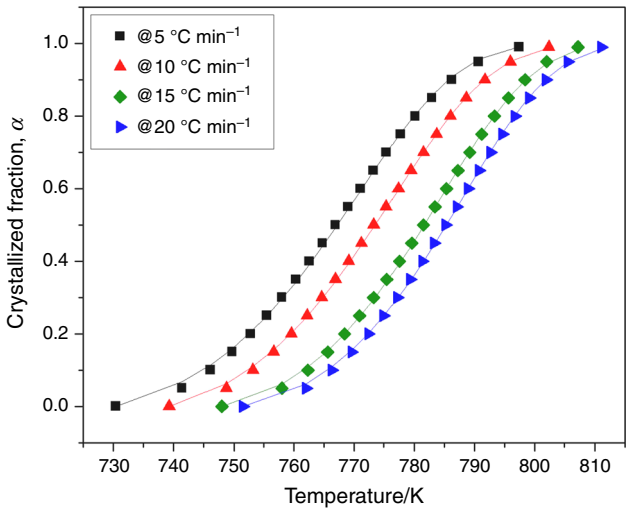

Fig. 3 Variation in crystallized fraction with temperature at different heating rates: *Symbols* represent experimental points, and *solid lines* show the least square fitted curve by Eq. (8)

Table 1 Values of Avrami (growth) exponent (n), pre-exponential factor (k_0), and activation energy (E) obtained by least square fitting of fractional crystallization data for second crystallization peak

Heating rates/°C min^{-1}	KJMA		
	n	k_0/s^{-1}	E/kJ mol^{-1}
5	1.09	3.66×10^{15}	264
10	1.13	2.8×10^{15}	260
15	1.22	2.08×10^{15}	258
20	1.26	2.28×10^{15}	258

$$y(\alpha) = \phi \exp(E/RT) \tag{9}$$

$$z(\alpha) = \phi T^2 \tag{10}$$

where ϕ is the heat flow evaluated during the crystal growth, represented by the following equation

$$\phi = \Delta H_c k_0 \exp(-E/RT) f(\alpha) \tag{11}$$

and

$$f(\alpha) = n(1-\alpha)[-\ln(1-\alpha)]^{(n-1)/n} \tag{12}$$

where ΔH_c is the enthalpy difference associated with crystallization process. The maximum of $y(\alpha)$ and $z(\alpha)$ is represented by α_M and α_p. In the present case, we have calculated both $y(\alpha)$ and $z(\alpha)$ as expressed in Eqs. (9) and (10), respectively. According to Malek, KJMA model is valid if the maximum value of $z(\alpha)$ function, i.e., α_P, lies between 0.61 and 0.65. Here, the value of α_P comes out to be in the range 0.57–0.66. Hence, KJMA model can be used to study the kinetic process (Fig. 4).

If $0 < \alpha_M < \alpha_P$, and α_P is not equal to zero, then the equation for $f(\alpha)$ given by Sestak–Berggren can be used for evaluating the kinetic parameters.

Sestak–Berggren (S–B) [37] equation is given as:

$$f(\alpha) = \alpha^M (1-\alpha)^N \tag{13}$$

where M and N are kinetic parameters, and their ratio can be calculated as:

$$\frac{M}{N} = \frac{\alpha_M}{(1-\alpha_M)} \tag{14}$$

Considering S–B equation, the reaction rate can be given as:

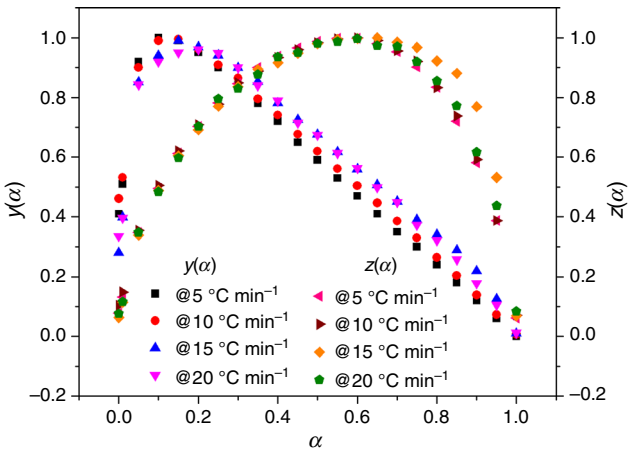

Fig. 4 Normalized $y(\alpha)$ and $z(\alpha)$ with crystallized fraction α for different heating rates

$$\frac{d\alpha}{dt} = Z\exp\left(-\frac{E_\alpha}{RT}\right)\alpha^{M}(1-\alpha)^{N} \quad (15)$$

Another way of representing S–B equation is:

$$\ln\left[\left(\frac{d\alpha}{dt}\right)\exp\left(\frac{E_\alpha}{RT}\right)\right] = \ln Z + N\ln[\alpha^{M/N}(1-\alpha)] \quad (16)$$

The value of N can be obtained from the slope of the plot $\ln[(d\alpha/dt)\exp(E_\alpha/RT)]$ versus $\ln[\alpha^{M/N}(1-\alpha)]$. Then, the parameter M can be calculated from Eq. (14).

After calculating value of M and N, S–B equation is obtained. Then, the so-obtained $f(\alpha)$ is used to plot the master curve. In master plot method [38], the $f(\alpha)$ is calculated at $\alpha = 0.5$, and then, theoretically calculated values of $f(\alpha)$ are reduced by dividing it by $f(0.5)$:

$$\frac{f(\alpha)}{f(0.5)} = \frac{d\alpha/dt}{(d\alpha/dt)_{0.5}}\frac{\exp(E_\alpha/RT)}{\exp(E_\alpha/RT_{0.5})} \quad (17)$$

The left-hand side of Eq. (17) represents the theoretical value of reaction model, whereas right-hand side represents the experimental values obtained from DSC data.

The master plots represented by Fig. 5 show the comparison between theoretical and experimental values of reduced $f(\alpha)$ with respect to $f(0.5)$. The trend followed by the theoretical models for all heating rates is same as the experimental results. The theoretical curves deviate from experimental curve at $\alpha = 0.1$. This deviation increases till $\alpha = 0.2$, and then, it decreases. The deviation of theoretical S–B curves from experimental curve decreases with increase in heating rate, while for JMA the deviation increases. At $\alpha = 0.5$, both curves match well with experimental curve till the end of the peak. Master plots confirm the validity of S–B model and JMA model for Zr-based metallic glass.

Further, theoretical normalized heat flow curves are obtained from Eqs. (11) and (12), using calculated kinetic parameters E and n, to check the applicability of KJMA model. From Fig. 6, it can be observed that at initial stage, the theoretical heat flow curve matches with experimental data. Both the reaction models superimpose the experimental heat flow curve at peak temperature for all the

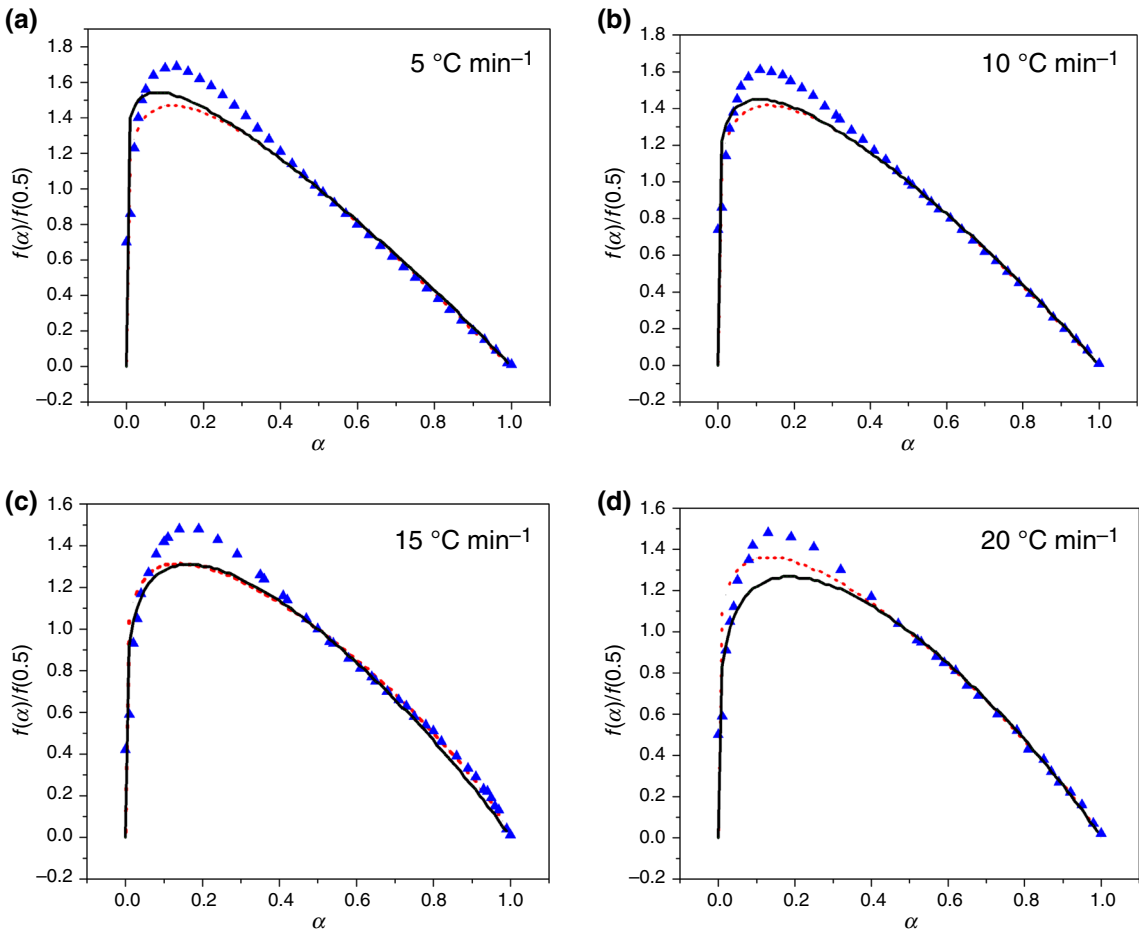

Fig. 5 Master plot at different heating rates; (*triangles*) experimental, (*solid line*) JMA, (*dotted line*) S–B: **a** @5 °C min^{-1}, **b** @10 °C min^{-1}, **c** @15 °C min^{-1}, **d** @20 °C min^{-1}

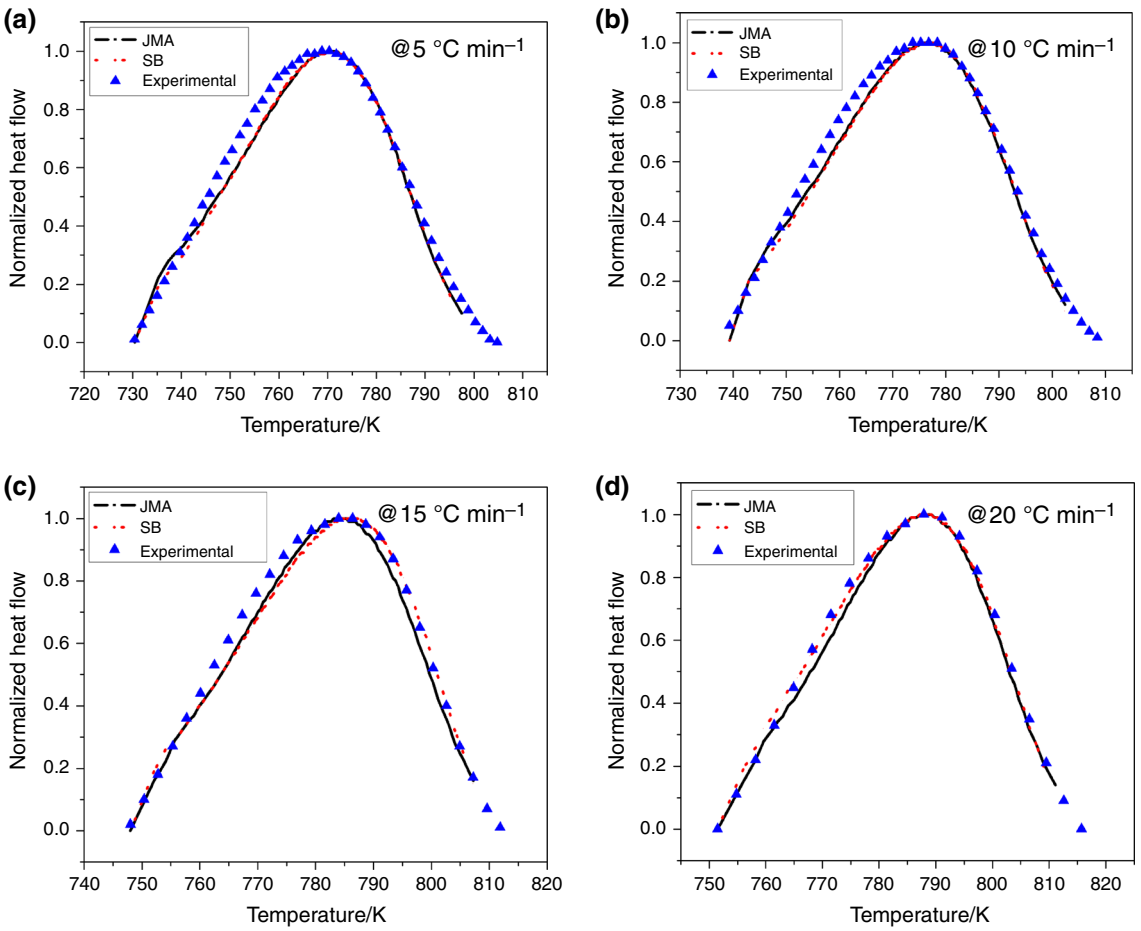

Fig. 6 Normalized heat flow curves at different heating rates. **a** @5 °C min^{-1}, **b** @10 °C min^{-1}, **c** @15 °C min^{-1}, **d** @20 °C min^{-1}

heating rates. After peak, the theoretical model provides a fairly good agreement with experimental data. Therefore, a good match between the theoretical heat flow curves with experimental data indicates that the crystallization kinetics for Zr-based system can be studied by both reaction models, i.e., KJMA and SB. As heating rate increases, the normalized heat flow curve obtained by SB reaction model exactly matches with the experimental data. Hence, to study the crystallization process, isokinetic methods are necessary. But, they provide single values of kinetic parameters, which is insufficient to understand entire crystallization process. So, isoconversional method which gives E depending on α is important. Hence, in the present case, the crystallization kinetics is studied by both isokinetic and isoconversional methods.

Isoconversional methods

Linear integral isoconversional methods

Kissinger–Akahira–Sunose (KAS) method To evaluate the temperature integral in Eq. (2), Kissinger–Akahira–Sunose (KAS) [2, 39] used the approximation given by Coats and Redfern [40], and hence derived the following equation:

$$\ln\left(\frac{\beta}{T_\alpha^2}\right) = -\frac{E_\alpha}{RT_\alpha} + \ln\left(\frac{k_0 R}{E_\alpha}\right) \tag{18}$$

The slope and intercept of $\ln(\beta/T_\alpha^2)$ versus $1000/T_\alpha$ plot provides the values of E_α and the k_0 for constant conversion, α (Fig. 7). Table 2 reports the values of local activation energies, E_α. Further special cases of KAS method are discussed.

(a) *Kissinger method* Kissinger equation is based on the assumption that the rate of reaction is highest at peak temperature (T_p). It calculates activation energy at a constant degree of conversion, α, i.e., at $T_\alpha = T_p$ only.

$$\ln\left(\frac{\beta}{T_p^2}\right) = -\frac{E}{RT_p} + \ln\left(\frac{k_0 R}{E}\right). \tag{19}$$

The slope and intercept of the $\ln(\beta/T_p^2)$ versus $1000/T_p$ plot gives the values of activation energy, E, and

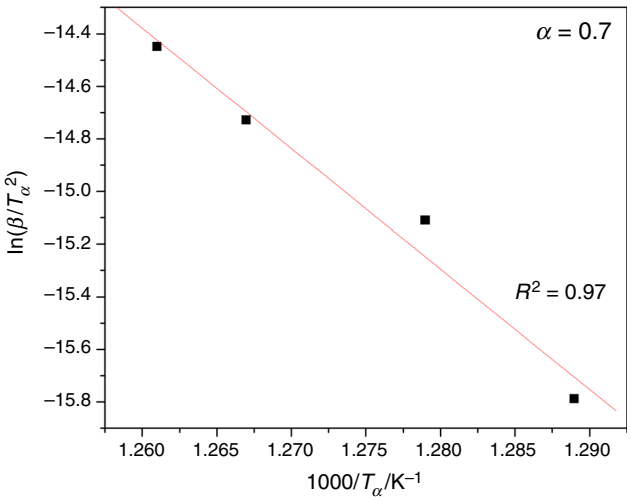

Fig. 7 KAS plot for $\alpha = 0.7$

Table 2 Local activation energies (E_α) at different degrees of conversions, α for different methods

A	E_α/kJ mol^{-1}		
	KAS	OFW	Friedman
0.1	265 ± 5	290 ± 5	328 ± 6
0.2	310 ± 6	307 ± 5	355 ± 6
0.3	322 ± 5	320 ± 5	356 ± 6
0.4	329 ± 6	327 ± 6	376 ± 6
0.5	346 ± 7	344 ± 7	394 ± 7
0.6	364 ± 7	360 ± 7	413 ± 7
0.7	381 ± 7	376 ± 6	439 ± 6
0.8	403 ± 8	398 ± 8	484 ± 7
0.9	448 ± 6	441 ± 7	531 ± 6

the pre-exponential factor (k_0), respectively. k_0 is the frequency factor, i.e., the number of jumps required by an atom to overcome the barrier, and forms stable nuclei. The value of E and k_0 is given in Table 3. This method is independent of reaction order and has very less dependence on the thermal history of the material (Fig. 8).

Table 3 Activation energy (E) and pre-exponential factor (k_0) for different methods

Methods	E/kJ mol^{-1}	k_0/s^{-1}
Kissinger	308 ± 8	4.77×10^{15}
Augis and Bennett	324 ± 10	2.56×10^{19}
Boswell	314 ± 8	–
Ozawa	311 ± 8	–
Gao and Wang	357 ± 9	–

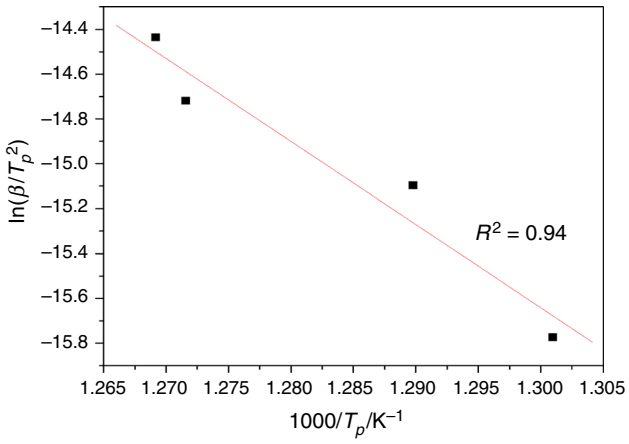

Fig. 8 Kissinger plot

(b) *Augis and Bennett's method* This method is a modification of Kissinger equation in which peak temperature (T_p) along with onset temperature of crystallization (T_o) is used [41]. This method is applicable to heterogeneous reactions.

$$\ln\left(\frac{\beta}{(T_p - T_o)}\right) = -\frac{E}{RT_p} + \ln(k_0) \tag{20}$$

The values of E and k_0 calculated, respectively, from the slope and intercept of the plot $\ln(\beta/(T_p - T_o))$ versus $1000/T_p$ (Fig. 9) are given in Table 3.

(c) *Boswell method* Boswell method [42] was formulated to overcome the limitations of Augis and Bennett method. As $((T_p - T_o)/T_p) \approx 1$, Augis and Bennett methods may provide crude results. This method determines the activation energy at peak temperature, shown in Table 3.

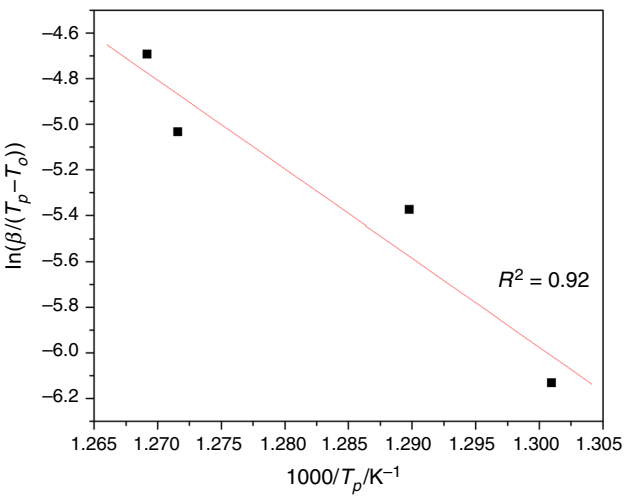

Fig. 9 Augis and Bennett's plot

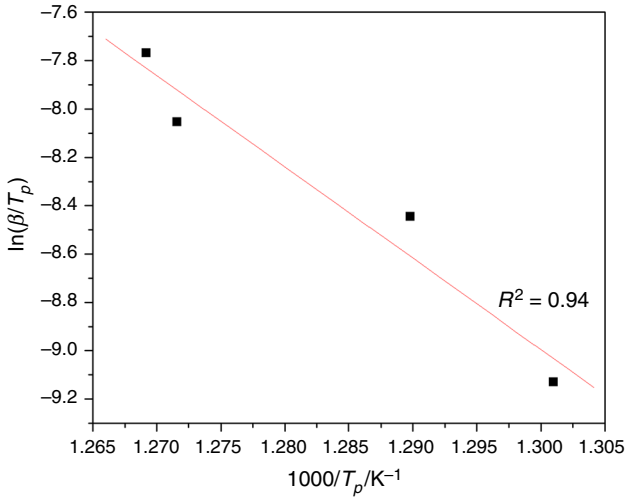

Fig. 10 Boswell plot

$$\ln\frac{\beta}{T_{\mathrm{p}}} = -\frac{E}{RT_{\mathrm{p}}} + \text{const} \tag{21}$$

The value of E as calculated from the slope of the plot $\ln(\beta/T_{\mathrm{p}})$ versus $1000/T_{\mathrm{p}}$ (Fig. 10) is 314 kJ mol^{-1} for peak-2.

Ozawa–Flynn–Wall (OFW) In OFW [43, 44] method, Doyle's approximation [45–47] is used to simplify the temperature integral in Eq. (2) which is approximated to be equal to $(-E/RT)$:

$$\ln\beta = -1.0516\frac{E_\alpha}{RT_\alpha} + \text{Const} \tag{22}$$

The plot $\ln(\beta)$ versus $1000/T_\alpha$ for constant conversion, α, is shown in Fig. 11 for peak 2. The values of E_α are reported in Table 2. At peak crystallization temperature, i.e., $T_\alpha = T_{\mathrm{p}}$, the value for activation energy is determined using Eq. (22) for Ozawa method. This method involves the substitution of T_{p} for T_α in Eq. (22). The value of E calculated from Ozawa method is reported in Table 3 (Fig. 12).

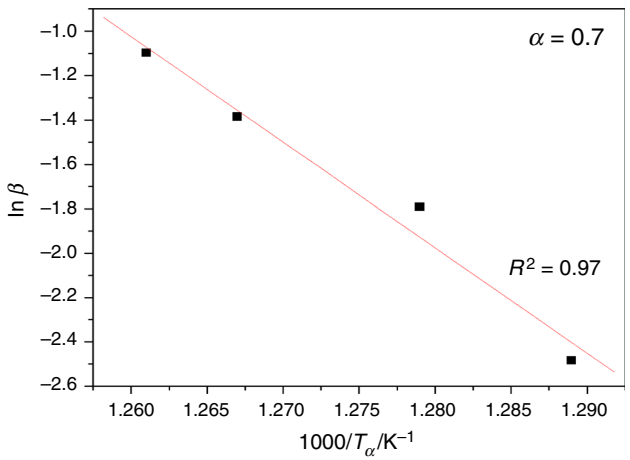

Fig. 11 OFW plot for α = 0.7

Linear differential isoconversional methods

Friedman method Friedman [48] derived an expression for estimation of activation energy of crystallization based on the differential of the transformed fraction. Since it does not require any approximation for temperature integral, accurate results of E are expected to be obtained. The expression given by Friedman is as follows:

$$\ln\left(\frac{\mathrm{d}\alpha}{\mathrm{d}t}\right)_\alpha = \ln\beta\left(\frac{\mathrm{d}\alpha}{\mathrm{d}T}\right)_\alpha = -\frac{E_\alpha}{RT_\alpha} + \ln(k_0 f(\alpha)) \tag{23}$$

Since it is a differential method, so its accuracy depends upon signal noise. The values of E_α calculated from the slope of the plot $\ln(\beta(\mathrm{d}\alpha/\mathrm{d}T)_\alpha)$ versus $1000/T_\alpha$ for constant conversion, α (Fig. 13), are given in Table 2.

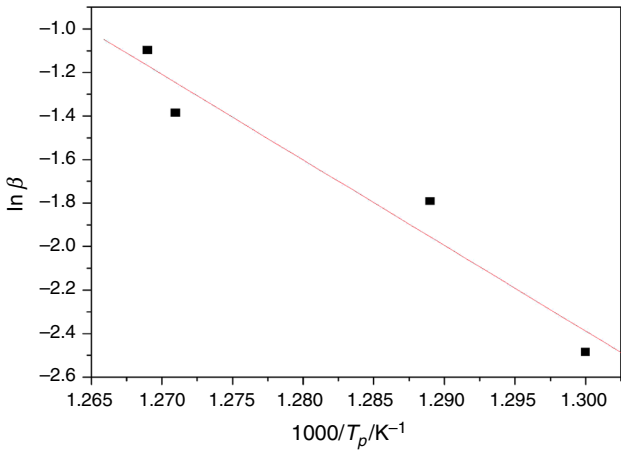

Fig. 12 Ozawa plot

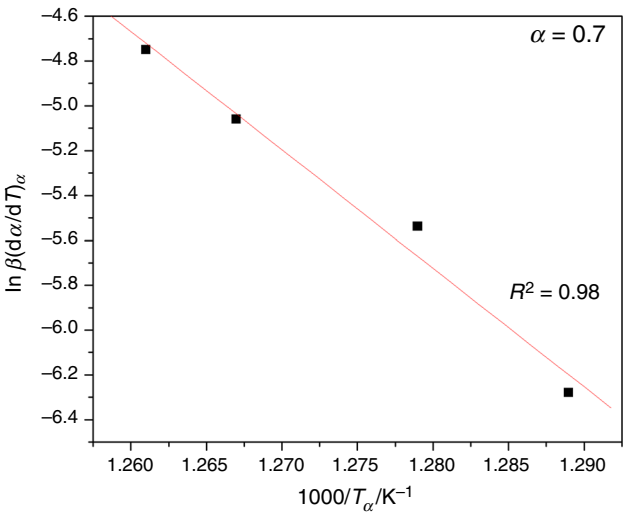

Fig. 13 Friedman plot for α = 0.7

A special case of Friedman method, which involves the determination of E only at T_p, was suggested by Gao and Wang [49]. This model is based on the assumption of random nucleation and site saturation. The expression used by Gao and Wang is as follows:

$$\ln\left(\beta\frac{d\alpha}{dT_p}\right) = -\frac{E}{RT_p} + \text{Const} \quad (24)$$

The values of E can be calculated from the slope of the plot $\ln(\beta(d\alpha/dT_p))$ versus $1000/T_p$. The values are given in Table 3 (Fig. 14).

It is observed that E values for second step of crystallization are greater than that of first step, by all the models. This indicates that secondary crystallization requires more energy for overcoming the barrier and forming stable nuclei. In general, it is observed that activation energy for first peak is higher compared to second peak [50, 51], indicating that the primary phase transition has modified the matrix and secondary crystallization has become easier. But for the present case, it is observed that activation energy for first peak [33] is lower than second peak. For $Co_{69}Fe_3Si_{18}B_{10}$ metallic glass [50], the values of E for first and second step are 370 and 327 kJ mol^{-1}, respectively, by Kissinger method. But for the present case, E values are found to be 259 and 308 kJ mol^{-1} for first and second peaks, respectively. Also, the activation energy increases rapidly for second peak. For the first peak, it was found to increase from 264 to 303 kJ mol^{-1}, whereas for the second peak, it increases from 265 to 448 kJ mol^{-1} by KAS method.

In Fig. 15, variation in local activation energies (E_α) with crystallized fraction (α) for peak 2 is shown by three different methods, i.e., KAS, OFW, and Friedman. The value of activation energies is reported in Table 2. It can be observed that values of E_α obtained by KAS and OFW

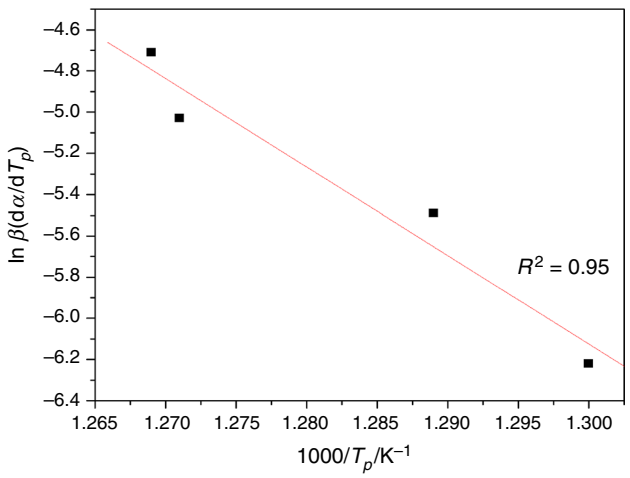

Fig. 14 Gao and Wang plot

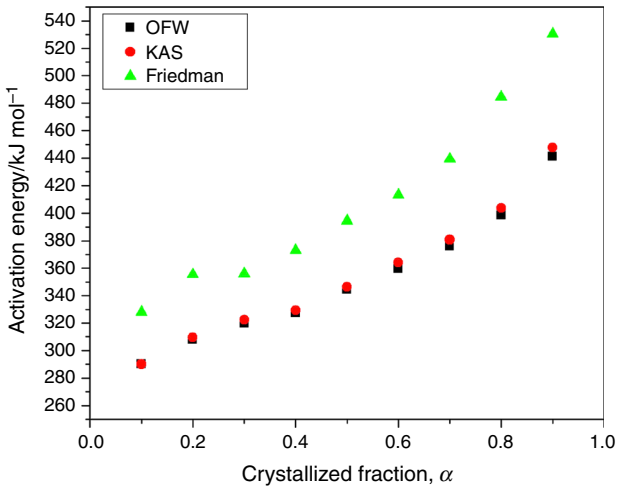

Fig. 15 Local activation energies (E_α) at different α from different methods

methods lie close to each other. As observed from Fig. 15, the values of local activation energy of crystallization constantly increase with the crystallized fraction α. This increase in E_α may be understood in terms of decrease in free volume of crystal due to the presence of primary crystallites. The formation of secondary crystallite takes place on primary crystallites. For the growth of secondary crystallites, the atoms are required to move through the melt which faces a barrier due to the presence of primary crystallites and decreasing free volume. As a result of which the activation energy E_α for secondary crystallization increases with increase in α, at a higher rate as compared to primary crystallization.

Isokinetic methods

Matusita and Sakka method

Matusita and Sakka [52] gave the following expression for studying the non-isothermal crystallization kinetics of metallic glasses.

$$\ln[-\ln(1-\alpha)] = -n\ln\beta - \frac{mE}{RT} + \text{Const} \quad (25)$$

where the integer m defines the dimensionality of the crystal, and the Avrami exponent n gives information about the nucleation process. The value of n can be obtained from the slope of the plot of $\ln[-\ln(1-\alpha)]$ versus $\ln\beta$, at a constant temperature. Further, the slope of the plot $\ln[-\ln(1-\alpha)]$ versus $1000/T$ at a constant heating rate gives the value of m. The value of m for second crystallization peak is 1.32. This implies that secondary crystallization proceed through one-dimensional growth of nuclei. Table 4 represents the values of Avrami exponent (n) and

Table 4 Values of Avrami exponent (n) and dimensionality (m) by Matusita and Sakka method

Heating rates/ °C min^{-1}	Value of Avrami exponent (n)	Dimensionality (m)
5	2.22	1.22
10	2.27	1.27
15	2.37	1.37
20	2.43	1.43

dimensionality (m) calculated by Matusita and Sakka method. It can be noticed that the value of n increases with increasing heating rates, indicating a higher particle density at higher heating rates (Figs. 16, 17).

For the non-isothermal crystallization, the local Avrami exponent can be calculated from the following equation [53]:

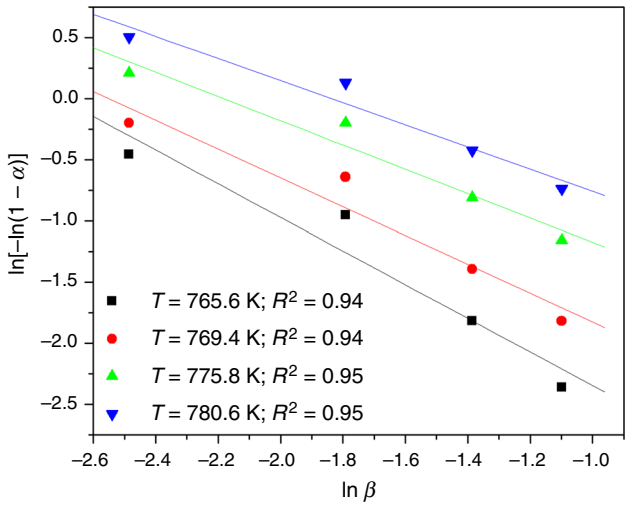

Fig. 16 Plot of ln[−ln(1 − α)] versus ln β

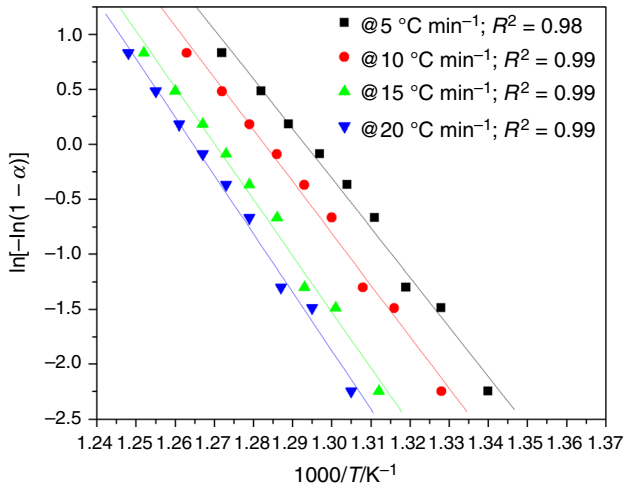

Fig. 17 Plot of ln[−ln(1 − α)] versus 1000/T for different heating rates

$$n(\alpha) = -\frac{R}{E(\alpha)}\frac{\mathrm{d}(\ln(-\ln(1-\alpha)))}{\mathrm{d}(1/T)} \tag{26}$$

Figure 18 represents the variation in local Avrami exponent with crystallized fraction at constant heating rate of 5 °C min^{-1}. It can be observed from this figure that the value of $n(\alpha)$ decreases with an increase in α, indicating that the transformation rate of crystalline particles decreases throughout the crystallization process. Similar behavior is observed at all heating rates.

Modified Kissinger method

The modified Kissinger [54] equation is expressed as:

$$\ln\left(\frac{\beta^{n}}{T_{p}^{2}}\right) = -\frac{mE}{RT_{p}} + \text{Const} \tag{27}$$

The slope of $\ln(\beta^{n}/T_{p}^{2})$ versus $1000/T_{p}$ gives the value of activation energy of crystallization. In this approach, the determination of the parameters m and n becomes important for the determination of E. Here, $m = n - 1$, and the value of n is obtained from Matusita and Sakka method. The value of E obtained is 269 kJ mol^{-1} (Fig. 19).

Effect of heating rate on primary and secondary crystallization processes

Primary crystallization process for $Zr_{52}Cu_{18}Ni_{14}Al_{10}Ti_{6}$ metallic glass was analyzed by Patel and Pratap [33]. The value of Avrami growth exponent (n) was found to be 2.66, which indicates that surface crystallization occurs in primary step of crystallization process. In the second step of crystallization, the value of Avrami exponent indicates diffusion-controlled crystallization process.

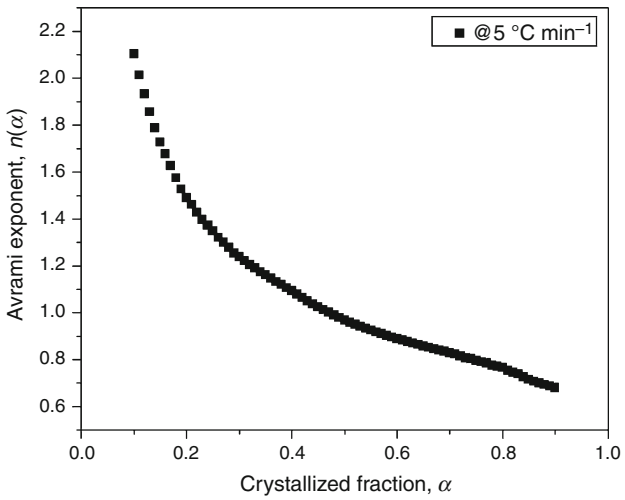

Fig. 18 Variation in local Avrami exponent with crystallized fraction

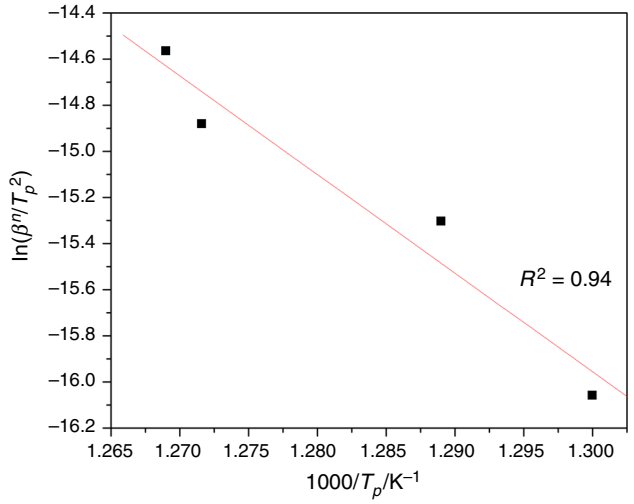

Fig. 19 Modified Kissinger plot

Figure 20 shows the variation in characteristic temperatures, i.e., onset and peak crystallization (T_x and T_p, respectively), for peak 1 and peak 2, with heating rate.

Lasocka's relation [55] was used to study the relationship between temperature and heating rate.

$$T = A + B \ln \beta \tag{28}$$

where A and B are constants. Least square method was used to obtain the values of A and B. The value of B indicates sensitivity toward heating rate. The values of constants A and B are reported in Table 5. From the table, it can be observed that the value of slope for peak 2, i.e., secondary crystallization, is greater than primary crystallization. The value of B for T_{x2} is largest, whereas it is smallest for T_{p1}. Hence, secondary crystallization is more sensitive toward heating treatment.

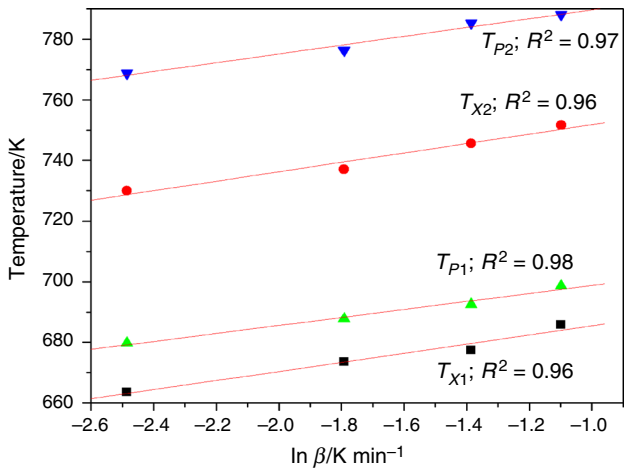

Fig. 20 Relationship between temperature and ln β for T_{x1}, T_{x2}, T_{p1}, and T_{p2}

Table 5 Values of A and B for $Zr_{52}Cu_{18}Ni_{14}Al_{10}Ti_6$ metallic glass

Constants	T_{x1}	T_{p1}	T_{x2}	T_{p2}
A	700 ± 4	712 ± 2	767 ± 4	804 ± 3
B	15 ± 2	13 ± 1	16 ± 2	14 ± 2

Conclusions

The second peak in curve which represents secondary crystallization was investigated to understand complete crystallization process. A criterion given by Malek and master plot method suggests that JMA model is applicable for kinetic studies. Further, normalized heat flow curve was examined to check the validity of JMA and SB models for studying kinetic process. The results indicate that both models lie in close agreement with experimental data at higher heating rates. Since, to understand the entire crystallization process, the information of value of E at different α is necessary, both routes for studying non-isothermal crystallization were followed. The non-isothermal crystallization kinetics for $Zr_{52}Cu_{18}Ni_{14}Al_{10}Ti_6$ metallic glass was studied by both isokinetic and isoconversional methods. Isokinetic methods provide the single value of activation energy E with Avrami exponent that gives the dimensionality of crystal growth. Isoconversional methods provide the activation energy E_α depending on different values of α. Hence, crystallization which is complex process can be well understood by both methods. Different kinetic parameters obtained by both methods for studying crystallization kinetics provide good result in the entire range. All the methods satisfactorily explains the variation in E_α with α. The activation energies obtained by KAS, OFW, and Friedman show an increasing trend with α. The increase in E_α with α may be due to decrease in free volume, which provides hindrance in diffusion of atoms toward stable configuration. The value of Avrami exponent decreases with α, indicating decrease in nucleation rate. The sensitivity of the characteristic temperatures toward heating rate is more for secondary crystallization event as compared to the primary crystallization event.

Acknowledgements The authors (Sonal Prajapati and Supriya Kasyap) are grateful to the Department of Science & Technology (DST), Govt. of India, for providing financial assistance under the DST-INSPIRE and DST-PURSE fellowship scheme, respectively.

References

1. Blazquez JS, Conde CF, Conde A. Non-isothermal approach to isokinetic crystallization processes: application to the nanocrystallization of HITPERM alloys. Acta Mater. 2005;53:2305–11.
2. Kissinger HE. Reaction kinetics in differential thermal analysis. Anal Chem. 1957;29:1702–6.

3. Ozawa T. Nonisothermal kinetics and generalized time. Thermochim Acta. 1986;100:109–18.
4. Mahadevan S, Giridhar A, Singh AK. Calorimetric measurements on As–Sb–Se glasses. J Non-Cryst Solids. 1986;88:11–34.
5. Soltan AS. Calorimetric study of the chalcogenide glass $Se_{77}Te_{20}Sb_3$. Phys B. 2001;307:78–85.
6. Afify N. A new method to study the crystallization or chemical reaction kinetics using thermal analysis technique. J Phys Chem Solids. 2008;69:1691–7.
7. Li JF, Huang ZH, Zhou YH. Crystallization of amorphous $Zr_{60}Al_{15}Ni_{25}$ alloy. Intermetallics. 2007;15:1013–9.
8. Jiang JZ, Zhuang XY, Rasmussen H, Saida J, Inoue A. Formation of quasicrystals and amorphous-to-quasicrystalline phase transformation kinetics in $Zr_{65}Al_{7.5}Ni_{10}Cu_{7.5}Ag_{10}$ metallic glass under pressure. Phys Rev B. 2001;64:094208.
9. Cai AH, An WK, Luo Y, Li TL, Li XS, Xiong X, Liu Y. Glass forming ability, non-isothermal crystallization kinetics, and mechanical property of $Zr_{61.5}Al_{10.7}Cu_{13.65}Ni_{14.15}$ metallic glass. J Alloys Compd. 2010;490:642–6.
10. Gao YL, Shen J, Sun JF, Wang G, Xing DW, Xian HZ, Zhou BD. Crystallization behavior of ZrAlNiCu bulk metallic glass with wide supercooled liquid region. Mater Lett. 2003;57:1894–8.
11. Xing PF, Zhuang YX, Wang WH, Gerward L, Jiang JZ. Glass transition, crystallization kinetics and pressure effect on crystallization of ZrNbCuNiBe bulk metallic glass. J Appl Phys. 2002;91:4956–60.
12. Jang JSC, Chang LJ, Chen GL, Huang JC. Crystallization behavior of the $Zr_{63}A_{17.5}Cu_{17.5}Ni_{10}B_2$ amorphous alloy during isothermal annealing. Intermetallics. 2005;13:907–11.
13. Lad KN, Savalia RT, Pratap A, Dey GK, Banerjee S. isokinetic and isoconversional study of crystallization kinetics of a Zr-based metallic glass. Thermochim Acta. 2008;473:74–80.
14. Qiao JC, Pelletier JM. Isochronal and isothermal crystallization in $Zr_{55}Cu_{30}Ni_5Al_{10}$ bulk metallic glass. Trans Nonferrous Met Soc China. 2012;22:577–84.
15. Prashanth KG, Scudino S, Surreddi KB, Sakaliysa M, Murty BS, Eckert J. Crystallization kinetics of $Zr_{65}Ag_5Cu_{12.5}Ni_{10}Al_{7.5}$ glassy powders produced by ball milling of pre-alloyed ingots. Mater Sci Eng, A. 2009;513–514:279–85.
16. Lu X, Li H, Xiao P, Wu R, Li D. The kinetic analysis of the non-isothermal crystallization process of $(Zr_{46}Cu_{42}Al_7Y_5)_{95}Be_5$ metallic glass. Thermochim Acta. 2013;570:27–32.
17. Kasyap S, Patel A, Pratap A. Crystallization kinetics of $Ti_{20}Cu_{60}Zr_{20}$ metallic glass by isoconversional methods using modulated differential scanning calorimetry. J Therm Anal Calorim. 2014;116:1325–36.
18. Paulik F. Ch. 10: Special trends in thermal analysis. Chichester: Wiley; 1995.
19. Vyazovkin S, Wight CA. Model-free and model-fitting approaches to kinetic analysis of isothermal and nonisothermal data. Thermochim Acta. 1999;340–341:53–68.
20. Burnham AK, Dinh LN. A comparison of isoconversional and model-fitting approaches to kinetic parameter estimation and application predictions. J Therm Anal Calorim. 2007;89(2):479–90.
21. Starink MJ. The determination of activation energy from linear heating rate experiments: a comparison of the accuracy of isoconversion methods. Thermochim Acta. 2003;404:163–76.
22. Vyazovkin S, Dollimore D. Linear and nonlinear procedures in isoconversional computations of the activation energy of non-isothermal reactions in solids. J Chem Inf Comput Sci. 1996;36(1):42–5.
23. Pratap A, Rao TLS, Lad KN, Dhurandhar HD. Isoconversional *vs.* model fitting methods. J Therm Anal Calorim. 2007;89(2):399–405.
24. Pacurariu C, Lazau I. Non-isothermal crystallization kinetics of some glass-ceramics with pyroxene structure. J Non-Cryst Solids. 2012;358:3332–7.
25. Kolmogorov AN. On the statistical theory of the crystallization of metals. Bull Acad Sci USSR Phys Ser. 1937;3:355–9.
26. Johnson WA, Mehl PA. Reaction kinetics of nucleation and growth. Trans Am Inst Min Metall Eng. 1939;135:416–32.
27. Avrami M. Kinetics of phase change. I: General theory. J Chem Phys. 1939;7(12):1103–12.
28. Avrami M. Kinetics of phase change. II Transformation-time relations for random distribution of nuclei. J Chem Phys. 1940;8(2):212–24.
29. Avrami M. Granulation, phase change, and microstructure kinetics of phase change III. J Chem Phys. 1941;9(2):177–84.
30. Mohan NS, Chen R. Numerical curve fitting for calculating glow parameters. J Phys D Appl Phys. 1970;3:243–9.
31. Tang W, Liu Y, Zhang H, Wang C. New approximation formula for Arrhenius temperature integral. Thermochim Acta. 2003;408:39–43.
32. Gorbachev VM. A solution of the exponential integral in the non-isothermal kinetics for linear heating. J Therm Anal. 1975;8:349–50.
33. Patel AT, Pratap A. Kinetics of crystallization of $Zr_{52}Cu_{18}Ni_{14}Al_{10}Ti_6$ metallic glass. J Therm Anal Calorim. 2012;107:159–65.
34. Johari GP, Schmelzer JWP. Crystal nucleation and growth in glass forming systems: some new results and open problems. In: Schmelzer JWP, editor. Glass: selected properties and crystallization. New York: Walter de Gruyter; 2014. p. 521–87.
35. Zhuang YX, Duan TF, Shi HY. Calorimetric study of non-isothermal crystallization kinetics of $Zr_{60}Cu_{20}Al_{10}Ni_{10}$ bulk metallic glass. J Alloys Compd. 2011;509:9019–25.
36. Malek J. The applicability of Johnson–Mehl–Avrami model in the thermal analysis of the crystallization kinetics of glasses. Thermochim Acta. 1995;267:61–73.
37. Sestak J, Berggren G. Study of the kinetics of the mechanism of solid-state reactions at increasing temperatures. Thermochim Acta. 1971;3:1–12.
38. Gotor FJ, Criado JM, Malek J, Koga N. Kinetic analysis of solid-state reactions: The universality of master plots for analyzing isothermal and non-isothermal experiments. J Phys Chem A. 2000;104:10777–82.
39. Akahira T, Sunose T. Joint convention of four electrical institutes. Research report (Chiba Institute of Technology). Sci Technol. 1971;16:22–31.
40. Coats AW, Redfern JP. Kinetic parameters from thermo-gravimetric data. Nature (Lond). 1964;201:68–9.
41. Augis A, Bennett JE. Calculation of Avarami parameters for heterogeneous solid state reactions using modification of the Kissinger method. J Therm Anal Calorim. 1978;13:283–92.
42. Boswell PG. On the calculation of activation energies using modified Kissinger method. J Therm Anal Calorim. 1980;18:353–8.
43. Ozawa T. A new method for analyzing thermogravimetric data. Bull Chem Soc Jpn. 1965;38:1881–6.
44. Flynn JH, Wall LA. General treatment of the thermogravimetry of polymers. J Res Natl Bur Stand A Phys Chem. 1966;70A:487–523.
45. Doyle CD. Kinetic analysis of thermogravimetric data. J Appl Polym Sci. 1961;5:285–92.
46. Doyle CD. Estimating isothermal life from thermogravimetric data. J Appl Polym Sci. 1962;6:642–93.
47. Doyle CD. Series approximation to the equation of thermogravimetric data. Nature (Lond). 1965;207:290–1.
48. Friedman HL. Kinetics of thermal degradation of char-forming plastics from thermogravimetry. J Polym Sci. 1964;C6:183–95.

49. Gao YQ, Wang W. On the activation energy of crystallization in metallic glasses. J Non-Cryst Solids. 1986;81:129–34.
50. Srivastava AP, Srivastava D, Mazumdar B, Dey GK. Thermo-analytical study of crystallization process in metallic glass of $Co_{69}Fe_3Si_{18}B_{10}$. J Therm Anal Calorim. 2015;119:1353–61.
51. Zhang Z, Wang WH, Hirotsu Y. Glass forming ability and crystallization behaviour of $Nd_{60}Al_{10}Ni_{10}Cu_{20-x}Fe_x$ (x = 0, 2, 4) bulk metallic glass with distinct glass transition. Mater Sci Eng, A. 2004;385:38–43.
52. Matusita K, Sakka S. Kinetic study of crystallization of glass by differential scanning calorimetry. Phys Chem Glasses. 1979;20:81–4.
53. Lu W, Yan B, Huang WH. Complex primary crystallization kinetics of amorphous Finemet alloy. J Non-Cryst Solids. 2005;351:3320–4.
54. Matusita K, Sakka S. Kinetic study of crystallization of glass by differential thermal analysis—criterion on application of Kissinger plot. J Non-Cryst Solids. 1980;38–39:741–6.
55. Lasocka M. The effect of scanning rate on glass transition temperature of splat-cooled $Te_{85}Ge_{15}$. Mater Sci Eng. 1975;23:173–7.

Bull. Mater. Sci., Vol. 38, No. 7, December 2015, pp. 1693–1698. © Indian Academy of Sciences.

A thermodynamic approach towards glass-forming ability of amorphous metallic alloys

SONAL R PRAJAPATI, SUPRIYA KASYAP and ARUN PRATAP*

Condensed Matter Physics Laboratory, Applied Physics Department, Faculty of Technology and Engineering, The M. S. University of Baroda, Vadodara 390001, India

MS received 31 May 2014; accepted 7 August 2015

Abstract. **A quantitative measure of the stability of a glass as compared to its corresponding crystalline state can be obtained by calculating the thermodynamic parameters, such as the Gibbs free energy difference (ΔG), entropy difference (ΔS) and the enthalpy difference (ΔH) between the super-cooled liquid and the corresponding crystalline phase. ΔG is known as the driving force of crystallization. The driving force of crystallization (ΔG) provides very important information about the glass-forming ability (GFA) of metallic glasses (MGs). Lesser the driving force of crystallization more is the GFA. The ΔG varies linearly with the critical size (d_c). According to Battezzati and Garonne the parameter $\gamma (= (1-(\Delta H_x/\Delta H_m))/(1-(T_x/T_m)))$ in the expression for ΔG should be a constant (i.e., 0.8), but its uniqueness is not observed for all MGs. The thermal stability of various alloy compositions is studied by their undercooled liquid region ($\Delta T = T_x - T_g$). Large ΔT_x implies greater stability against crystallization of the amorphous structure. Other GFA parameters are also calculated and correlated with critical size (d_c).**

Keywords. **Metallic glass; Gibbs free energy; critical size.**

1. Introduction

Metallic alloys can be converted into metallic glasses by cooling their melt at a high rate, i.e., 10^5–10^6 K s^{-1}, such that their molecules does not get sufficient time to occupy stable configuration, thereby suppressing their crystallization event. These supercooled metallic alloys with a disordered atomic scale arrangement and connected by metallic bonds are known as 'metallic glasses (MGs)'. Metallic alloys which fail to crystallize during solidification even at low critical cooling rate, i.e., less than 100 K s^{-1}, form 'bulk metallic glasses (BMGs)' with thickness ranging from 1 mm to several centimetres due to smaller cooling rates. MGs and BMGs are prepared by different synthesis routes. Melt spinning technique is used to prepare amorphous ribbons of metallic alloys, which involves rapid cooling. On the other hand, BMGs are formed by different methods such as copper mould casting, arc melting, which require comparatively low cooling rate. These metastable materials possess excellent properties, such as high strength, high hardness, exhibit good corrosion resistance and attractive soft magnetic behaviour.[1,2] This inspires us to study the thermal properties of MGs in the undercooled region. To design an alloy having excellent glass-forming ability (GFA), many empirical approaches have been proposed based on trial and error experiments,[3–5] but there are no justified theories and scientific rules. The GFA of alloys may be characterized by the Gibbs free energy difference (ΔG). Decreasing ΔG acts as a driving force for nucleation causing an increase in critical nucleation work and a reduction in nucleation rate. Lele *et al*[6] studied the temperature dependence of free energy of crystallization. It provides an insight for understanding the effect of heating rate on nucleation in undercooled region. The value of ΔG can be calculated by the measurement of specific heat difference ΔC_p, which is difficult to attain experimentally. So, different theoretical approximations of ΔC_p results in a variety of expressions of ΔG.[7,8] To understand glass formation and to predict GFA, Guo *et al*[9] have imposed physically accepted boundary conditions to evaluate the GFA criteria, and performed statistical analysis in order to identify the best GFA criterion. Recently, Tang *et al*[10] have studied the GFA of Ce-based alloys, using different GFA parameters.

All GFA parameters are correlated with in order to interpret its sensitivity towards the GFA of MGs. Senkov[11] introduced GFA parameter based on fragility of MG and found a good correlation with critical cooling rate. Also Xiu-lin and Ye[12] formulated a new GFA parameter based on thermodynamic analysis and found a good correlation with d_c for Ca-Mg-Cu BMGs. In the present work, ΔG and other GFA parameters[5,13–16] for different MGs are calculated and are correlated with critical size to study the GFA of metallic alloys. ΔG is evaluated by different theoretical expressions. We have calculated ΔG to understand the glass formability of various MGs, i.e., $Ca_{50}Mg_{25}Cu_{25}$,[17] $Mg_{65}Cu_{25}Y_{10}$,[18,19] $Mg_{65}Cu_{20}Zn_5Y_{10}$,[20] $Mg_{59.5}Cu_{22.9}Ag_{6.6}Gd_{11}$,[21,22] $Fe_{41}Co_7Cr_{15}Mo_{14}C_{15}B_6Y_2$,[23,24] $Zr_{41.2}Ti_{13.8}Cu_{12.5}Ni_{10}Be_{22.5}$,[24,25] $Zr_{65}Cu_{17.5}Ni_{10}Al_{7.5}$,[24,26,27] $Pd_{40}Ni_{40}$

*Author for correspondence (apratapmsu@yahoo.com)

P_{20},[24,26,28] $Pd_{40}Ni_{10}Cu_{30}P_{20}$,[24,26,29] and $Au_{76.9}Ge_{13.65}Si_{9.45}$[28,30] by different expressions.

2. Theory

The general equation for ΔG between the undercooled liquid and corresponding crystalline phase is given by

$$\Delta G = \Delta H - T\Delta S \tag{1}$$

$$\Delta H = \Delta H_{\mathrm{m}} - \int_{T}^{T_{\mathrm{m}}} \Delta C_{\mathrm{p}} \mathrm{d}T \tag{2}$$

$$\text{and} \quad \Delta S = \Delta S_{\mathrm{m}} - \int_{T}^{T_{\mathrm{m}}} \Delta C_{\mathrm{p}} \frac{\mathrm{d}T}{T} \tag{3}$$

Where, ΔS_{m}, ΔH_{m} and T_{m} are the entropy, enthalpy and temperature of fusion, respectively. They are related to each other by the relation:

$$\Delta S_{\mathrm{m}} = \Delta H_{\mathrm{m}}/T_{\mathrm{m}} \tag{4}$$

So the equation becomes,

$$\Delta G = \Delta S\,(T_{\mathrm{m}} - T) - \int_{T}^{T_{\mathrm{m}}} \Delta C_{\mathrm{p}} \mathrm{d}T + T \int_{T}^{T_{\mathrm{m}}} \Delta C_{\mathrm{p}} \mathrm{d}(\ln T)$$

Turnbull[5] assumed ΔC_{p} to be zero. So ΔG can be written as

$$\Delta G = \Delta H_{\mathrm{m}} \left(\frac{\Delta T}{T_{\mathrm{m}}}\right). \tag{5}$$

Assuming $\Delta C_{\mathrm{p}} =$ constant, one gets

$$\Delta G = \Delta S_{\mathrm{m}}\,(T_{\mathrm{m}} - T) + \Delta C_{\mathrm{p}} \left[T \ln\left(\frac{T_{\mathrm{m}}}{T}\right) - (T_{\mathrm{m}} - T)\right].$$

To simplify the above equation, Thompson and Spaepen[7] (T–S) used the following approximation:

$$\ln \frac{T_{\mathrm{m}}}{T} \cong \frac{2\Delta T}{T_{\mathrm{m}} + T}.$$

And they derived an expression given as

$$\Delta G = \frac{\Delta H_{\mathrm{m}} \Delta T}{T_{\mathrm{m}}} \left(\frac{2T}{T_{\mathrm{m}} + T}\right). \tag{6}$$

This equation is only valid for small ΔT, and leads to error in calculations of ΔG values at larger undercooling.

Generally, multicomponent MGs exhibit larger undercooling range. Hence, equation (6) cannot be used for a wide range of MGs.

Lad *et al*[8] assumed $\Delta C_{\mathrm{p}} = \Delta H_{\mathrm{m}}/T_{\mathrm{m}}$ and used Taylor series expansion of $\ln(T_{\mathrm{m}}/T) = \ln(1 + \Delta T/T) = \Delta T[1 - \Delta T/2T]/T$, retaining terms up to second order and derived the expression:

$$\Delta G = \frac{\Delta H_{\mathrm{m}} \Delta T}{T_{\mathrm{m}}} \left(1 - \frac{\Delta T}{2T}\right) \text{[Lad-I]} \tag{7}$$

Again, considering Taylor series expansion of $\ln(T_{\mathrm{m}}/T) = \ln(1 + \Delta T/(T_{\mathrm{m}} + T)/2)$ and retaining up to second-order terms, i.e., $\ln(T_{\mathrm{m}}/T) = 4T\Delta T/(T_{\mathrm{m}} + T)^2$, Lad *et al*[31] gave the expression:

$$\Delta G = \frac{\Delta H_{\mathrm{m}} \Delta T}{T_{\mathrm{m}}} \left(\frac{4T^2}{(T + T_{\mathrm{m}})^2}\right) \text{[Lad-II]} \tag{8}$$

As stated by Hoffman[32]

$$\ln \frac{T_{\mathrm{m}}}{T} = 2\frac{T_{\mathrm{m}} - T}{T_{\mathrm{m}} + T}.$$

With this approximation equation becomes

$$\Delta G = \frac{\Delta H_{\mathrm{m}} \Delta T}{T_{\mathrm{m}}} \left(\frac{T}{T_{\mathrm{m}}}\right). \tag{9}$$

According to Battezatti and Garone[33] the expression for ΔG is given as follows:

$$\Delta G = \Delta S(T_{\mathrm{m}} - T) - \gamma \Delta S_{\mathrm{m}} \left[(T_{\mathrm{m}} - T) - T \ln(T_{\mathrm{m}}/T)\right]. \tag{10}$$

The γ-parameter in the above equation is represented as:

$$\gamma = \frac{(1 - \Delta H_x/\Delta H_{\mathrm{m}})}{(1 - \Delta T_x/\Delta T_{\mathrm{m}})}, \tag{11}$$

where ΔH_x denotes the enthalpy difference at crystallization.

Singh and Holz[34] (S and H) gave the following expression for linear variation of ΔC_{p} with T:

$$\Delta G = \frac{\Delta H_{\mathrm{m}} \Delta T}{T_{\mathrm{m}}} \left(\frac{7T}{T_{\mathrm{m}} + 6T}\right). \tag{12}$$

Ji and Pan[35] considered hyperbolic variation of ΔC_{p} with $T(\Delta C_{\mathrm{p}} = \Delta H_{\mathrm{m}}/T)$ and derived the following expression:

$$\Delta G = \frac{2\Delta H_{\mathrm{m}} \Delta T}{T_{\mathrm{m}}} \left(\frac{T}{T_{\mathrm{m}} + T} - \frac{\Delta T^2 T_{\mathrm{m}}}{3\,(T_{\mathrm{m}} + T)^3}\right). \tag{13}$$

Dubey and Ramchandrarao[36] derived expression for ΔG based on the hole theory of liquids given as:

$$\Delta G = \frac{\Delta H_{\mathrm{m}} \Delta T}{T_{\mathrm{m}}} - \frac{\Delta C_{\mathrm{p}}^{\mathrm{m}}\,(\Delta T)^2}{2T} \left(1 - \frac{\Delta T}{6T}\right). \tag{14}$$

Finally Lele *et al*[6] derived an expression of ΔG to study its temperature dependence for the entire undercooled region represented as:

$$\Delta G = \frac{\Delta H_{\mathrm{m}} \Delta T}{T_{\mathrm{m}}} - \frac{\Delta C_{\mathrm{p}}^{\mathrm{m}}\,(\Delta T)^2}{(T_{\mathrm{m}} + T)}. \tag{15}$$

3. Results and discussion

3.1 *Regression analysis*

The reliability of GFA criteria is evaluated by linear regression analysis and hence these criteria are correlated to their corresponding d_c. The GFA criterion is considered to be better if the coefficient of correlation R^2 is larger. The GFA parameters are calculated based on the available experimental data of characteristic temperatures, crystallization enthalpy and fusion enthalpy of BMGs in the literature. Critical size is a conclusive criterion for measuring GFA of BMGs. So d_c is related with other parameters to check whether these parameters can be used to evaluate the GFA. A statistical correlation factor, R^2 have been evaluated from the plots of d_c *vs.* GFA parameter for various BMGs. Higher the value of R^2, better is the correlation between d_c and GFA parameters. The value of R^2 can give idea about how efficient are the different GFA parameters to evaluate GFA of MGs. The value of R^2 determines the relationship between GFA criteria and d_c. It should reflect one-to-one correspondence between the two variables. If the value of R^2 is around unity, it is considered to be highly correlated and having exact linear relationship. The advantage of doing such a regression analysis lies in the fact that it provides consideration to select GFA criteria, and this study is useful to get a quantitative idea about how different GFA parameters reflect the GFA of different metallic alloys.

Figure 1a–d shows the plots of d_c *vs.* thermodynamic parameter ΔG, and other parameters T_{rg}, ΔT_x, Q, α, β, γ_m, respectively, for the BMGs listed in table 1. By using the linear regression method, a linear relationship can be obtained between d_c and GFA parameters. From the plots it can be observed that all GFA parameters show a correlation with d_c, indicating that all these parameters to a certain range reflect GFA of alloys. The values of correlation coefficient R^2 were computed to be 0.67 for the d_c–ΔG plot, 0.01, 0.58, 0.64, 0.53 for the d_c–Q, γ_m, α, β plots, 0.68 for d_c–T_{rg} plot and 0.32 for d_c–ΔT_x plot, respectively. From the values of R^2, it can be observed that ΔG, which is the driving force of crystallization and reduced glass transition temperature T_{rg}, better represents GFA of different MGs. $\Delta G(T_g)$ varies inversely with d_c and hence it shows a negative correlation with d_c. As $\Delta G(T_g)$ increases, d_c decreases and hence GFA decreases.

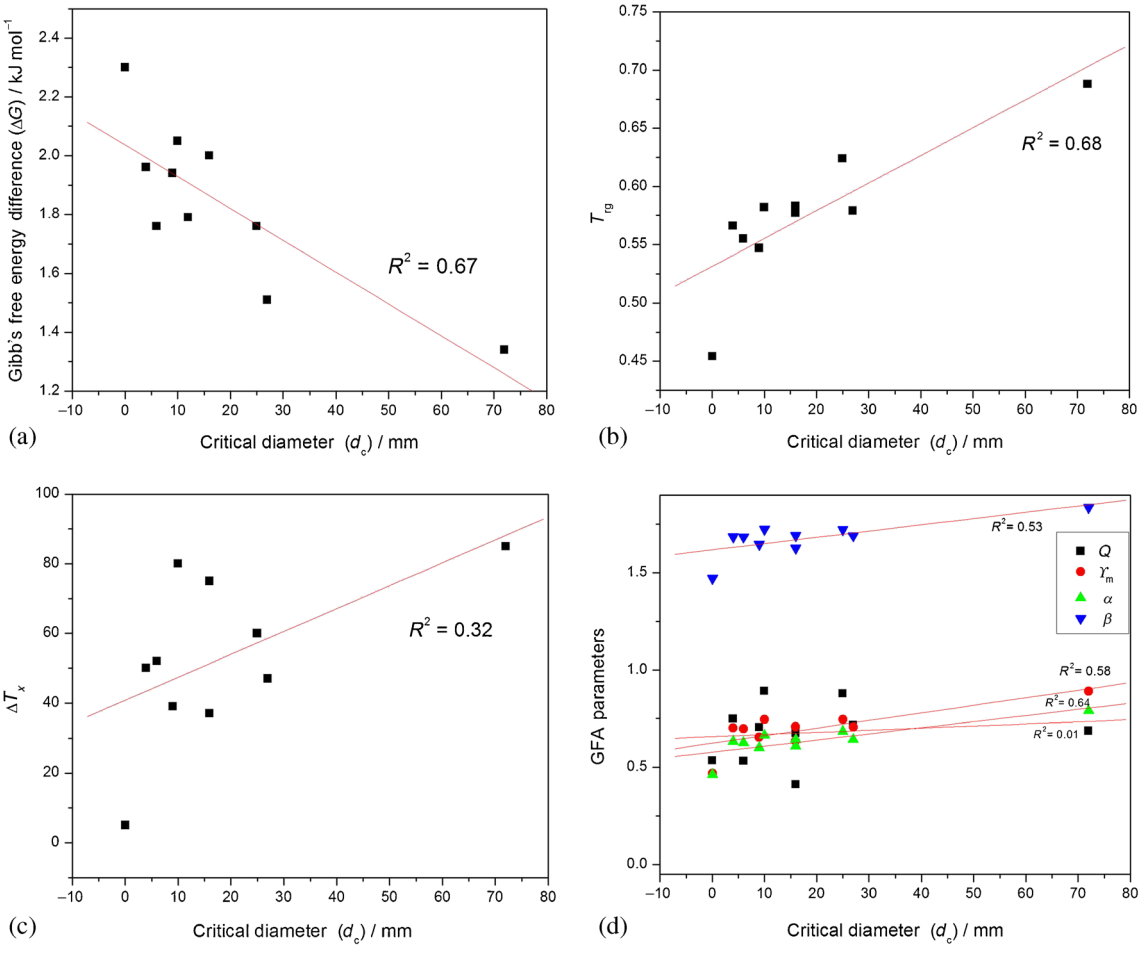

Figure 1. Variation of Gibb's free energy difference ΔG, T_{rg}, ΔT_x and other GFA parameters with critical diameter (d_c).

Table 1. Thermodynamic parameter ΔG by different theoretical expressions.

Systems	d_c (mm)	$\Delta G(T_g)$ by different expressions (kJ mol^{-1})								
		Lad-I	Lad-II	Hoffman	Turnbull	Ji and Pan	S and H	T and S	B and G	γ (equation 11)
$Ca_{50}Mg_{25}Cu_{25}$	9	2.287	1.938	2.037	3.193	2.424	2.954	2.487	2.339	1.29
$Mg_{65}Cu_{25}Y_{10}$	4	2.317	1.961	2.117	3.697	2.576	3.341	2.692	2.718	1.05
$Mg_{65}Cu_{20}Zn_5Y_{10}$	6	2.082	1.760	1.898	3.289	2.308	2.984	2.410	2.000	1.57
$Mg_{59.5}Cu_{22.9}Ag_{6.6}Gd_{11}$	27	1.791	1.515	1.599	2.555	1.912	2.354	1.967	1.805	1.35
$Fe_{41}Co_7Cr_{15}Mo_{14}C_{15}B_6Y_2$	16	2.375	2.004	2.134	3.535	2.572	3.232	2.661	2.087	1.78
$Zr_{41.2}Ti_{13.8}Cu_{12.5}Ni_{10}Be_{22.5}$	25	2.065	1.760	1.836	2.774	2.163	2.585	2.209	2.134	1.2
$Zr_{65}Cu_{17.5}Ni_{10}Al_{7.5}$	16	2.754	2.324	2.487	4.198	3.008	3.822	3.124	2.880	1.31
$Pd_{40}Ni_{40}P_{20}$	10	2.417	2.050	2.151	3.335	2.552	3.092	2.615	2.604	1.08
$Pd_{40}Ni_{10}Cu_{30}P_{20}$	72	1.536	1.337	1.373	1.905	1.576	1.805	1.596	0.994	3.09
$Au_{76.9}Ge_{13.65}Si_{9.45}$	0.04	2.466	2.302	2.642	5.597	3.263	4.826	3.589	4.124	0.8

Lower the value of ΔG, lesser will be the driving force of nucleation, which degrades the crystallization hence better will be the GFA. So thermodynamically the GFA of metallic alloys can be understood by $\Delta G(T_g)$. Other GFA parameters show a reasonable linear relation with d_c, except for T_{rg}. As T_{rg} increases GFA also increases and it shows a positive correlation with d_c. GFA of MG is considered to be high if the value of T_{rg} lies in the range 0.66–0.69. In the present case $Pd_{40}Ni_{10}Cu_{30}P_{20}$ has T_{rg} value of 0.68, indicating that it is a best glass former among all. The parameter α derived by Mondal and Murty[37] is independent of T_g, so for metallic alloys for which distinct T_g is not observed the GFA can be estimated which proves its applicability. The parameter Q is derived based on consideration of liquid-phase stability, resistance to crystallization and enthalpy of crystallization, which is heating rate dependent. So it may not be sufficient to study the GFA of metallic alloys. ΔT_x represents the stability of glass, i.e., how far is the crystallization from glass transition. A greater value of ΔT_x represents greater stability of glass against crystallization. But from figure 1c it can be seen that there exists a weak correlation between ΔT_x and d_c, which implies that GFA is not closely related to ΔT_x. d_c represents GFA of MGs, as d_c increases GFA increases. A good GFA parameter is expected to show one-to-one correspondence with d_c. So for the same value of d_c a good GFA parameter should have same values. But for the parameter ΔT_x few MGs with same value of d_c have different ΔT_x values. Although GFA and glass thermal stability are related properties, ΔT_x cannot be used to understand both of them. Weinberg[38] found that a high GFA does not always indicate a high thermal stability. Hence, GFA and thermal stability can be different for few MGs. Therefore ΔT_x cannot be used as a GFA parameter.

In the present case, correlation between GFA criteria and d_c gives lower value of R^2. This may be due to the fact that the compositions of metallic alloys used in this study are significantly different from each other. The MGs having slight variation in composition show high value of R^2. Cai *et al*[39] studied GFA of Zr-Al-Ni-Cu-based bulk MGs and found that GFA parameters show strong correlation with critical size.

From figure 1 it can be observed that different GFA parameters deviate from the fitted line. For some GFA criteria, the deviation from the fitted line is quite large as the regression analysis is based on dispersed data on different metallic systems.

The values of R^2 for α and β are found to be higher than that of ΔT_x, which imply that they are strongly correlated and better indicator of GFA. The weak correlation of ΔT_x is due to the fact that it can only reflect the stability of glass, whereas α and β combine both the properties i.e., thermal stability of glass and ease of glass formation. It is reported in literature that some glass-forming criteria such as ΔT_x and T_{rg} when correlated with R_c or d_c show a high degree of diversion in number of cases.[40,41] So analysing data which is highly distributed may not provide accurate results. The value of R^2 for the plots of different GFA parameter with d_c is not so high because d_c is also dependent on different casting conditions used by different researchers.

3.2 *Estimation of Gibbs free energy difference*

ΔG plays an important role in predicting GFA of metallic alloys. Driving force for crystal nucleation can be estimated by the calculation of a thermodynamic parameter, i.e., ΔG. The value of ΔG increases with lowering of temperature due to decrease in entropy of metallic alloy. It indicates that at lower temperature ample amount of driving force is available for crystallization. Hence, nucleation starts at lower temperature followed by the growth of crystal. As temperature increases growth of stable nuclei takes place. At glass transition temperature (T_g) the driving force is maximum, which allows the amorphous alloy to move towards crystallization. With further increase in temperature, ΔG approaches towards zero. Hence, crystallization event ends due to increase in entropy of the alloy resulting in melting of alloy. So estimation of ΔG at T_g becomes important to study the GFA of metallic alloys.

Table 2. Thermodynamic parameter ΔG for different metallic glasses.

Systems	$\Delta G(T_g)$ (kJ mol^{-1}) Experimental	$\Delta G(T_g)$ by different expressions (kJ mol^{-1}) Dubey and Ramchandrarao	Lele *et al*
$Mg_{65}Cu_{25}Y_{10}$	2.761	2.601	2.787
$Zr_{41.2}Ti_{13.8}Cu_{12.5}Ni_{10}Be_{22.5}$	2.190	2.361	2.414
$Pd_{40}Ni_{40}P_{20}$	2.953	2.573	2.677
$Pd_{40}Ni_{10}Cu_{30}P_{20}$	1.378	1.386	1.440
$Au_{76.9}Ge_{13.65}Si_{9.45}$	4.486	4.638	4.841

In the present case, $\Delta G(T_g)$ has been calculated by the various theoretical expressions given by Turnbull, T and S, S and H, Ji and Pan, Lad *et al*, Hoffman, Battezzati and Garonne. Here all expressions of ΔG are based on different temperature dependence of ΔC_p. All these expressions estimate $\Delta G(T_g)$ with minimum experimental data available. The calculated values of $\Delta G(T_g)$ are shown in table 1. Based on the experimental data available in literature for few MGs, it is observed from the above calculated values of $\Delta G(T_g)$ by different expressions that provide accurate values of ΔG at T_g for all systems. The experimental values of $\Delta G(T_g)$ for $Mg_{65}Cu_{25}Y_{10}$,[18] $Zr_{41.2}Ti_{13.8}Cu_{12.5}Ni_{10}Be_{22.5}$,[25] $Pd_{40}Ni_{40}P_{20}$,[28] $Pd_{40}Ni_{10}Cu_{30}P_{20}$[27] and $Au_{76.9}Ge_{13.65}Si_{9.45}$[28] are as shown in table 2. For $Pd_{40}Ni_{40}P_{20}$ the experimental results lie close to the values obtained by S and H expression, whereas for $Pd_{40}Ni_{10}Cu_{30}P_{20}$ alloy Hoffman and Lad-II expressions show better agreement. Also it was found that T and S as well as B and G provide good results for other BMGs. Hence, these expressions may give accurate results for few BMGs, but it may not be true for all the cases. So, one cannot predict which equation gives better results for evaluation of ΔG, for a wide range of MGs with different compositions. As stated by Battezzati and Garonne[33] the value γ should be equal to 0.8 for all MGs, but from the table 1 it can be observed that it varies for different MGs. The reason for variation of γ can be the difficulty to choose suitable crystallization step in multistep crystallization process for multicomponent MGs. Moreover T_x and ΔH_x are also heating rate dependent.[42] So γ cannot be considered as constant and it is calculated by using equation (11). There are some more expressions available in literature[43–45] to determine ΔG, which require more experimental parameters to obtain exact values.

Also thermodynamic analysis is carried out by the expressions of ΔG given by Lele *et al*[6] and Dubey and Ramchandrarao,[36] which are found to be in close agreement with the experimental results. The values of $\Delta G(T_g)$ as calculated by both expressions are shown in table 2.

The metallic alloy is considered to be a good glass former if the value of ΔG is low. Pd-based metallic alloys are found to have highest GFA, having minimum critical cooling rate.[46] Here the value of ΔG of $Pd_{40}Ni_{10}Cu_{30}P_{20}$ composition was found to be the lowest (= 1.378 kJ mol^{-1}) among all composition indicating its higher GFA.

4. Conclusion

Based on reasonably good correlation with d_c, thermodynamic parameter ΔG reflects the GFA of metallic alloys. ΔG shows a negative correlation with d_c, whereas other parameters show a positive correlation. The correlation of d_c with other parameters also shows linear dependence, suggesting that they are equally important to predict GFA of all MGs. T_{rg} also show a high correlation with d_c, hence it is a good GFA indicator. So thermodynamically the GFA of the metallic alloys can also be predicted and alloy with higher GFA can be designed. By comparing the values of GFA parameters of glass-forming alloys, one can conclude that $Pd_{40}Ni_{10}Cu_{30}P_{20}$ has high GFA among all as it has lowest value of ΔG and large stability against crystallization, indicated by greater value of ΔT_x (= 85 K).

Acknowledgement

SRP and SK are grateful to the Department of Science & Technology (DST), Government of India, for providing financial assistance under the DST-INSPIRE and DST-PURSE fellowship scheme, respectively.

References

1. Schuh C 2007 *Acta Mater.* **55** 4067
2. Ashby M F and Greer A L 2006 *Scr. Mater.* **54** 321
3. Inoue A 2000 *Acta Mater.* **48** 279
4. Inoue A, Zhang T and Masumoto T 1993 *J. Non-Cryst. Solids* **473** 156
5. Turnbull D 1969 *Contem. Phys.* **10** 473
6. Lele S, Dubey K S and Ramchandrarao P 1985 *Curr. Sci.* **54** 994
7. Thompson C V and Spaepen F 1979 *Acta Metall.* **27** 1855
8. Lad K N, Pratap A and Raval K G 2002 *J. Mater. Sci. Lett.* **21** 1419
9. Guo S, Lu Z P and Liu C T 2010 *Intermetallics* **18** 883
10. Tang C, Li Y, Pan W, Du Y, Xiong X, Zhou Q, Wang J and Zhou H 2012 *J. Non-Cryst. Solids* **358** 1368
11. Senkov O N 2007 *Phys. Rev. B* **76** 104202
12. Xiu-lin J and Ye P 2009 *Trans. Nonferrous Met. Soc. China* **19** 1271

13. Inoue A, Zhang T and Masumoto T 1990 *Mater. Trans. JIM* **31** 177
14. Du X H, Huang J C, Liu C T and Lu Z B 2007 *J. Appl. Phys.* **101** 086108
15. Yuan Z Z, Bao S L, Lu Y, Zhang D P and Yao L 2008 *J. Alloys Compd.* **459** 251
16. Suo Z Y, Qiu K Q, Li Q F, You J H, Ren Y L and Hu Z Q 2010 *Mater. Sci. Eng. A* **528** 429
17. Senkov O N, Scott J M and Miracle D B 2006 *J. Alloys Compd.* **424** 394
18. Busch R, Liu W and Johnson W L 1998 *J. Appl. Phys.* **83** 4134
19. Inoue A, Kato A, Zhang T, Kim S G and Masumoto T 1991 *Mater. Trans. JIM* **32** 609
20. Men H, Hu Z Q and Xu J 2002 *Scr. Mater.* **46** 699
21. Zheng Q, Xu J and Ma E 2007 *J. Appl. Phys.* **102** 113519
22. Ma H and Fecht H J 2008 *J. Mater. Res.* **23** 2816
23. Shen J, Chen Q J, Sun J F, Fan H B and Wang G 2005 *Appl. Phys. Lett.* **86** 151907
24. Li Y, Poon S J, Shiflet G J, Xu J, Kim D H and Loffler J F 2007 *MRS Bull.* **32** 624
25. Busch R, Kim Y J and Johnson W L 1995 *J. Appl. Phys.* **77** 4039
26. Lu I R, Willde G, Gorler G P and Willnecker R 1999 *J. Non-Cryst. Solids* **250–252** 577
27. Cai A H, Xiong X, Liu Y, Chem H, An W K, Li X S, Zhou Y and Luo Y 2008 *Eur. Phys. J. B* **64** 147
28. Haruyama O, Watanabe T, Yuki K, Horiuchi M, Kato H and Nishiyama N 2011 *Phys. Rev. B* **83** 064201
29. Myung W N, Bae H Y, Hwamg I S, Kim H G, Nishiyama N, Inoue A and Greer A L 2001 *Mater. Sci. Eng. A* **304–306** 687
30. Chen H S and Turnbull D 1968 *J. Chem. Phys.* **48** 2560
31. Lad K N, Raval K G and Pratap A 2004 *J. Non-Cryst. Solids* **334–335** 259
32. Hoffman J D 1958 *J. Chem. Phys.* **29** 1192
33. Battezzati L and Garonne E 1984 *Z. Metallk.* **75** 305
34. Singh H B and Holz A 1983 *Solid State Commun.* **45** 985
35. Ji X L and Pan Y 2007 *J. Non-Cryst. Solids* **353** 2443
36. Dubey K S and Ramchandrarao P 1984 *Acta Metall.* **32** 91
37. Mondal K and Murty B S 2005 *J. Non-Cryst. Solids* **351** 1366
38. Weinberg M C 1994 *J. Non-Cryst. Solids* **167** 81
39. Cai A H, Xiong X, Liu Y, An W K, Tan J Y and Pan Y 2009 *J. Alloys Compd.* **468** 432
40. Lu Z P and Liu C T 2002 *Acta Metall.* **50** 3501
41. Lu Z P and Liu C T 2003 *Phys. Rev. Lett.* **91** 11
42. Dhurandhar H, Shankar Rao T L, Lad K N and Pratap A 2008 *Philos. Mag. Lett.* **88** 239
43. Jones D and Chadwick G 1971 *Philos. Mag.* **24** 995
44. Singh P K and Dubey K S 2012 *Ther. Chim. Acta* **530** 120
45. Li P, Wang G, Dong D and Shen J 2013 *J. Alloys Compd.* **550** 221
46. Nishiyama N and Inoue A 2002 *Mater. Trans.* **43** 1913

International Conference on Ceramics, Bikaner, India
International Journal of Modern Physics: Conference Series
Vol. 22 (2013) 327–331

DOI: 10.1142/S2010194513010301

STUDY OF GLASS FORMING ABILITY PARAMETERS OF Mg-Ni-Pr-BASED METALLIC GLASSES*

SONAL R. PRAJAPATI

Condensed Matter Physics Laboratory, Applied Physics Department,
Faculty of Technology and Engineering, The M.S.University of Baroda
Vadodara, Gujarat-390001, India
sonal051987@yahoo.in

ASHMI T. PATEL

Condensed Matter Physics Laboratory, Applied Physics Department,
Faculty of Technology and Engineering, The M.S.University of Baroda
Vadodara, Gujarat-390001, India
ashmi0707@yahoo.co.in

ARUN PRATAP

Condensed Matter Physics Laboratory, Applied Physics Department,
Faculty of Technology and Engineering, The M.S.University of Baroda
Vadodara, Gujarat-390001, India
apratapmsu@yahoo.com

Knowledge of Glass forming Ability (GFA) of metallic glasses is of great importance as it gives an insight of a better Glass former. Number of GFA parameters like Gibb's free energy difference ΔG, ΔS, ΔH, η, γ, γ_m, Q, T_{rg} ($=T_g/T_l$) etc. are calculated and compared for Mg-Ni-Pr-based metallic glass forming alloys to predict which parameter describes the best GFA criterion. On the basis of these parameters the excellent glass forming composition is identified. Also the GFA parameters of Mg-Ni-Pr-based alloys are studied in air and argon atmosphere. Present work suggests that ΔG is the best GFA criterion and Mg-Ni-Pr-based metallic glassy alloys can be successfully fabricated in air due to its high oxidation resistance ability.

Keywords: Bulk Metallic Glasses, Gibb's Free Energy, GFA.

Introduction

Bulk metallic glasses have found significant interest in research as it has many applications. Various parameters and criteria have been proposed to predict GFA. Glass formation is a competition process between super-cooled liquid and the related crystalline phases.[1] In order to find better glass forming metallic glass many theoretical approaches have been put forward through criteria like reduced glass transition temperature(T_{rg}), order parameter(η), parameters Q, γ, γ_m, and the Gibb's Free energy difference (ΔG) between the super-cooled liquid and crystalline phases. A large number of systems follow these all criteria with some exceptions. The driving force of nucleation is given by

thermodynamic factor i.e. Gibb's free energy difference ΔG. Lower the value of ΔG lesser will be the driving force of nucleation which degrades the crystallization hence better will be the GFA.[2]

In the present work different GFA criteria for Mg-Based metallic alloys with different composition and in different atmosphere are calculated. The thermodynamic properties like ΔG and ΔS are also determined.

Formulation of Theoretical Expression

The Gibbs free energy difference gives a qualitative measure of the stability of the glass compared to the crystalline state. The difference in Gibbs free energy between the liquid and crystalline phases is given by

$$\Delta G = \Delta H - T\Delta S. \tag{1}$$

Where,
$$\Delta H = \Delta H_m - \int_T^{T_m} \Delta C_p dT \,. \tag{2}$$

And

$$\Delta S = \Delta S_m - \int_T^{T_m} \Delta C_p \frac{dT}{T} \tag{3}$$

Where, T_m is the melting temperature, ΔS_m is the entropy of fusion and ΔH_m is the enthalpy of fusion. They are related to each other by the following relation:

$$\Delta S_m = \frac{\Delta H_m}{T_m}. \tag{4}$$

ΔC_p, defined as $C_p^{\,l} - C_p^{\,x}$, is the difference in specific heat of liquid and the corresponding crystalline phases of metallic alloy. The most common linear expression is given by

$$\Delta C_p = AT + B. \tag{5}$$

Substituting Eq. (5) in Eqs. (2) and (3), Eq. (1) can be simplified to

$$\Delta G = \frac{\Delta H_m \Delta T}{T_m} - \frac{1}{2} A(\Delta T)^2 + B\left(T \ln \frac{T_m}{T} - \Delta T \right). \tag{6}$$

Considering large undercooled region of the multicomponent metallic alloys Lad et al.[3] obtained the following expression.

$$\Delta G = \frac{\Delta H_m \Delta T}{T_m}\left(1 - \frac{\Delta T}{2T}\right). \tag{7}$$

Considering logarithmic term in eq. (6) and taking the Taylor series expansion up to second order gives the following approximation:

$$\ln\left(\frac{T_m}{T}\right) \cong \frac{4T\Delta T}{(T + T_m)^2}. \tag{8}$$

Substituting Eq. (8) in Eq. (6) Lad et al.[4] obtained the following equation for the Gibb's free energy difference

$$\Delta G = \frac{\Delta H_m \Delta T}{T_m}\left(\frac{4T^2}{(T+T_m)^2}\right). \tag{9}$$

The entropy difference can be obtained by taking partial derivative of ΔG w.r.t to t:

$$\Delta S = -\frac{\partial(\Delta G)}{\partial T}. \tag{10}$$

Substituting Eq. (7) & (9) in (10) we get the following equation,

$$\Delta S_1 = \frac{\Delta H_m}{2T_m}\left(\frac{3T^2 - T_m^{\,2}}{T^2}\right). \tag{11}$$

$$\Delta S_2 = \frac{4\Delta H_m T}{T_m}\left(\frac{T^2 - 2T_m^2 + 3TT_m}{(T+T_m)^3}\right). \tag{12}$$

Results and Discussion

Many criteria have been predicted for finding the GFA of metallic glasses like $\gamma_m(=2T_x-T_g/T_l)$, $Q(=(T_g+T_x)/T_l)$, η $(=1-\Delta H_x/\Delta H_m)$, $\gamma(=T_x/(T_g+T_l))$, $T_{rg}(=T_g/T_l)$ etc. where, T_l, T_x, T_g are liquidus, crystallization, and glass transition temperature respectively. All parameters are calculated in Table-1 which shows that T_{rg}, γ, γ_m gives constant value which cannot give idea about variation in GFA for the given compositions. One can see that there is a significant variation in ΔG values which can predict better glass forming composition. ΔG is the driving force for crystallization. Lower the value of ΔG, higher is the GFA of metallic alloys.

Table 1. Different GFA Criteria

Systems.[5]	ΔTx (K).[5]	Q	T_{rg}[5]	η	γ [5]	γ_m	$\Delta G_1(T_g)$ (Lad-1) kJ/mol	$\Delta G_2(T_g)$ (Lad-2) kJ/mol	$\Delta G_1(T_g)$ $/\Delta H_m$	$\Delta G_2(T_g)$ $/\Delta H_m$	$\Delta S_1(T_g)$ (Lad-1) kJ/mol	$\Delta S_2(T_g)$ (Lad-2) kJ/mol
$Mg_{48}Ni_{31}Pr_{21}$	47	0.451	0.570	0.627	0.403	0.695	2.92	2.47	0.265	0.249	1.77	1.45
$Mg_{63}Ni_{22}Pr_{15}$	52	0.803	0.574	0.339	0.407	0.708	1.35	1.14	0.265	0.224	0.53	0.51
$Mg_{65}Ni_{21}Pr_{14}$	42	0.907	0.569	0.238	0.396	0.675	1.38	1.17	0.264	0.224	0.91	0.72
$Mg_{65}Ni_{21}Pr_{14}$ (air)	41	0.814	0.574	0.322	0.397	0.678	1.50	1.26	0.265	0.223	0.93	0.75

ΔG is calculated for the entire undercooled region, from Lad-1 &Lad-2 equations. Figure -1 shows ΔG variation with temperature for $Mg_{48}Ni_{31}Pr_{21}$ and $Mg_{63}Ni_{22}Pr_{15}$ metallic glasses. Lower the value of $\Delta G(T_g)$ indicates better GFA and hence $Mg_{63}Ni_{22}Pr_{15}$ is better glass former.

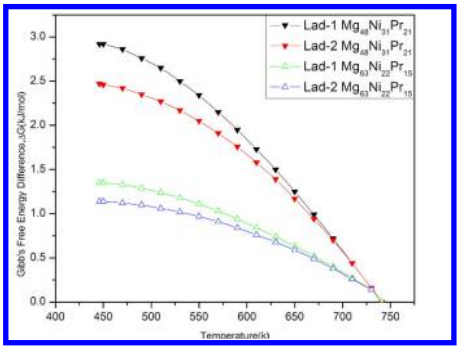

Figure 1. Gibb's free energy difference with Temperature for $Mg_{48}Ni_{31}Pr_{21}$ and $Mg_{63}Ni_{22}Pr_{15}$

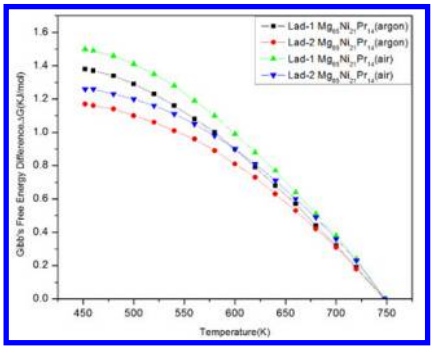

Figure 2. Gibb's free energy difference with Temperature for $Mg_{65}Ni_{21}Pr_{14}$ in air and argon atmosphere.

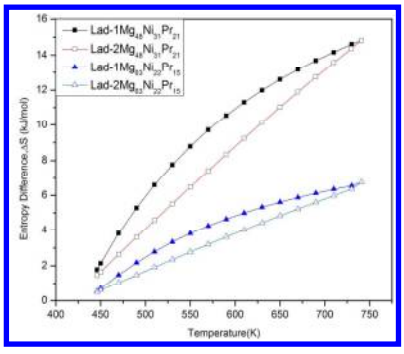

Figure 3. Entropy Difference with Temperature for $Mg_{63}Ni_{22}Pr_{15}$ and $Mg_{48}Ni_{31}Pr_{21}$.

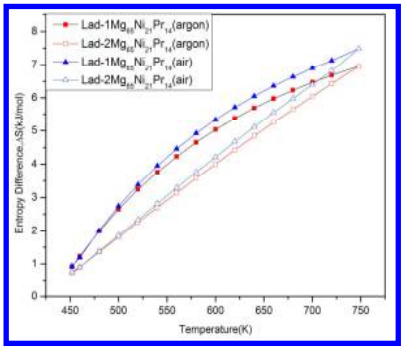

Figure 4. Entropy Difference with Temperature for $Mg_{65}Ni_{21}Pr_{14}$ in air and argon atmosphere.

Lower value of ΔG (T_g) indicates higher GFA and hence $Mg_{63}Ni_{22}Pr_{15}$ is better glass former. Lad-2 gives smaller value of $\Delta G(T_g)$ than Lad-1 for both the systems as given in table-1 which indicates that it is good approximation.$Mg_{65}Ni_{21}Pr_{14}$ metallic glass produced in argon is better glass former than $Mg_{65}Ni_{21}Pr_{14}$ produced in air as $\Delta G(T_g)$ is lower for sample prepared in argon as shown in figure-2. Mg-Ni-Pr system has high oxidation resistance ability so it can be prepared in air but for other BMGs it is not possible as in air they favour crystallization. The entropy difference, ΔS, between the undercooled liquid and the corresponding crystalline phase has also been calculated from Eq. (11) &(12), and plotted in fig. (3) & (4), for all the four composition i.e. $Mg_{48}Ni_{31}Pr_{21}$, $Mg_{63}Ni_{22}Pr_{15}$, $Mg_{65}Ni_{21}Pr_{14}$, $Mg_{65}Ni_{21}Pr_{14}$ (air).

Conclusion

It can be concluded that $Mg_{63}Ni_{22}Pr_{15}$ is the best glass former among all composition as the driving force of crystallization; ΔG is very low for it which indicates excellent GFA.

$Mg_{65}Ni_{21}Pr_{14}$ though has better GFA in argon atmosphere, but it can also be successfully prepared in air which is not possible for synthesis of other BMG's. ΔG value for $Mg_{65}Ni_{21}Pr_{14}$ metallic glass which is prepared in air has comparatively smaller value of ΔG (T_g) which indicates that $Mg_{65}Ni_{21}Pr_{14}$ is also a good glass former.

References

1. Z.Y.Suo, K.Q.Qui, Q.F.Li, J.H.You, Y.L.Ren, Z.Q.Hu, *Mater. Science & Engg.* A, 528(2010), 429-433
2. A.T.Patel, K.N.Lad, Arun Pratap, *Solid State Phen.*,171(2011) ,121-126
3. K.N.Lad,Arun Pratap,K.G.Raval, *J.Mater. Science Lett.*,21(2002), 1419-1422
4. K.N.Lad, K.G.Raval, Arun Pratap, *J.Non-Cryst. Solid,* 334&335(2004), 259-262
5. Y.X.Wei, X.K.Xi, D.Q.Zhao, M.X.Pan, W.H.Wang, *Mater.Lett*. 59 (2005), pp. 945-974

J Therm Anal Calorim (2017) 127:2083–2091
DOI 10.1007/s10973-016-5824-9

Effect of driving force of crystallization on critical cooling rate for Pd-based metallic glasses

Sonal R. Prajapati[1] · Supriya Kasyap[1] · Arun Pratap[1]

Received: 3 March 2016 / Accepted: 4 September 2016 / Published online: 21 September 2016

Abstract The advent of bulk metallic glasses (BMG) has opened lot of scope of wide range of applications for this class of amorphous materials. Thermodynamics plays a very important role in glass formation in multicomponent metallic alloys. BMG's can be synthesized with relatively lower cooling rate with ease now. However, the glass formation in these systems seems to depend on quite a few parameters like enthalpy of melting, reduced glass transition temperature, under cooling. In present paper, we have studied the glass forming ability of Pd-based metallic glasses using theoretically determined Gibbs free energy difference (ΔG), between the supercooled liquid and the corresponding crystalline phase, and the critical cooling rate (R_c). Time–temperature-transformation (TTT) diagrams were constructed to calculate R_c using Uhlmann and Davies formulation. Different theoretical expressions of ΔG are incorporated in nucleation and growth equations to find R_c from TTT diagram. The results obtained theoretically by Dhurandhar et al. expression of ΔG, assuming hyperbolic variation of specific heat difference (ΔC_p), were found to be in excellent agreement with experimental data for different Pd-based systems.

Keywords Bulk metallic glasses (BMG) · Glass forming ability (GFA) · Critical cooling rate (R_c) · Gibbs free energy difference · Time-temperature transformation (TTT) curves

The present article is based on the lecture presented at SATAC2014 conference in Dhanbad—India on 15–17 December, 2014.

✉ Sonal R. Prajapati
sonal051987@yahoo.in

Arun Pratap
apratapmsu@yahoo.com

[1] Condensed Matter Physics Laboratory, Applied Physics Department, Faculty of Technology and Engineering, The M. S. University of Baroda, Vadodara 390001, India

Introduction

The glass forming ability (GFA) is an open problem ever since the discovery of metallic glass. A metallic alloy can be transformed into glassy state provided that the melt can be undercooled to sufficiently low temperature and occurrence of crystallization is avoided. If cooling rate is high enough then less time will be available for molecules to arrange themselves and crystallization will not occur, hence glass formation will be favored. Scientific efforts have made to predict GFA of metallic alloys, thermodynamically as well as kinetically, so that metallic glasses with excellent GFA can be designed [1–3]. Thermodynamically, Gibbs free energy difference is a good indicator of GFA [4]. It is well known that the GFA of metallic alloy is expressed in terms of critical cooling rate (R_c) or critical size (Z_c). But Z_c is dependent on fabrication method rather than alloy composition [5]. So R_c is a ideal route to determine the GFA of metallic alloy. The experimental measurement of R_c involves series of continuous cooling experiments. To evaluate GFA by R_c for different alloy systems number of solidification trials with different cooling rates are necessary. So to estimate R_c theoretically, TTT curves are used. Rodova et al. [6] determined R_c of molten Zinc Chloride experimentally under isothermal and non-isothermal conditions, whereas theoretically R_c was determined using TTT curves. The calculation of R_c basically involves three factors [7]. (1) Computational model to calculate critical volume fraction crystallized, (2) expression to calculate nucleation and growth rate, (3) evaluation of several parameters used in nucleation and growth equations. From the knowledge of above criteria, theoretically R_c can be determined by TTT

curves. The TTT curve gives the time required to form volume fraction (X) of crystal during isothermal treatment. During solidification, crystallization occurs which is a two-step process i.e., nucleation and growth. Hence, TTT curves give the transformation of nucleation controlled to growth controlled crystallization [7]. This method is also known as "Nose method" [8]. It is observed that the nose method of predicting R_c is in reasonably good agreement with other methods [9].

R_c is the quantitative measure of the GFA, above which no crystallization occurs when melt is solidified. Also, lower R_c always corresponds to higher GFA [10]. The critical cooling rate (R_c) depends on three factors: nucleation rate and its temperature variation, crystal growth rate and its temperature dependence and relationship between the two quantities and volume fraction (X) [8].

Many studies have been reported to evaluate GFA for Pd-based metallic glasses [11, 12]. Nishiyama et al. [13] reported that $Pd_{40}Cu_{30}P_{20}Ni_{10}$ have high GFA with low critical cooling of 0.1 K s^{-1} for glass formation and maximum size is about 72 mm by water quenching technique. Also Xu et al. [14] demonstrated that the accurate experimental determination of some parameters, which are crucial for calculating R_c, is difficult. So they have drawn some random values of parameters and using the classical theory examined probabilistic distribution of R_c for Pd-based metallic glasses. Kim et al. [15] evaluated R_c for different metallic glasses by combining continuous cooling transformation (CCT) and continuous heating transformation (CHT) curves. More recently Xu et al. [16] have calculated R_c for Fe-based metallic alloy by Ulhmann [5] and Barandiaran–Colmenero method. In Ulhmann method, different expressions of ΔG and different models of viscosity [$\eta(T)$] were examined and it was found that R_c obtained by Thompson–Spaepen (TS) [17] expression for ΔG was in accordance with the experimental result. Ge et al. [18] have used Davies Uhlmann kinetic formulation to construct TTT curves of Cu-Zr binary alloys and found that R_c obtained using TS equation for ΔG gives better results than Turnbull equation.

In this study, the determination of R_c for the glass formation for Pd-based alloys is presented using TTT curves. Different theoretical models of ΔG in undercooled region of Pd-based metallic glasses are used and incorporating the so obtained values in nucleation and growth equations corresponding TTT curves are constructed. The main aim of this work is to reveal which expression for ΔG is suitable for determining R_c and how the variation in ΔG affects the value of R_c for glass formation of Pd-based alloys.

Theory

The volume fraction of crystallized material in an undercooled liquid alloy is very small so the critical volume fraction X can be expressed as [5, 19]:

$$X = \frac{\pi}{3} I_v u^3 t^4 \tag{1}$$

where I_v is the steady state nucleation rate, u is the crystal growth rate and t is the time taken for X to crystallize.

The I_v can be written as [20]

$$I_v = \frac{A}{\eta(T)} \exp\left(-\frac{\Delta G^*}{k_B T}\right) \tag{2}$$

where A is the fitting parameter given by the following equation:

$$A \approx \frac{N_A}{V_m} \frac{k_B T}{3\pi a_0^3} \tag{3}$$

with α_0 being the average atomic diameter and

$$\Delta G^*(T) = 16\pi\sigma^3/3[\Delta G(T)/V_m]^2 \tag{4}$$

where ΔG is the Gibbs free energy difference between liquid and crystalline phases, η is the temperature dependent viscosity of molten alloy, k_B is the Boltzman constant, V_m is the molar volume and σ (T) is the temperature dependent interfacial energy using the enthalpy of fusion given as [21]:

$$\sigma(T) = \frac{\alpha \Delta H_m}{\left(N_A V_m^2\right)^{1/3}} \frac{T}{T_m} \tag{5}$$

where $\alpha = 0.76$ for all Pd-based metallic systems.

For constructing TTT curve, the temperature dependence of viscosity (η) of Pd-based alloys is essential. The estimation of the viscosity for Pd-based alloys is based on Vogel–Fulcher–Tamman (VFT) equation:

$$\eta(T) = \eta_0 \exp\left(\frac{DT_0}{T - T_0}\right) \tag{6}$$

where η_0, D and T_0 are constants, which are necessary to be determined in order to obtain the expression of the viscosity.

The crystal growth u can be expressed by [22]:

$$u = f \frac{D}{a_0} \left[1 - \exp\left(-\frac{\Delta G}{RT}\right)\right] \tag{7}$$

where

$$D = \frac{k_B T}{3\pi a_0 \eta(T)} \tag{8}$$

with

$$f \approx 0.2(T_m - T)/T_m \tag{9}$$

So, to construct TTT diagram and to understand overall transformation kinetics of the amorphous alloys all parameters such as ΔG, σ, $\eta(T)$ need to be determined.

Estimation of the difference of Gibbs free energy between solid and liquid

The Gibbs free energy difference between the liquid and crystalline phases is given by

$$\Delta G = \Delta H - T\Delta S \tag{10}$$

where

$$\Delta H = \Delta H_{\mathrm{m}} - \int_{\mathrm{T}}^{T_{\mathrm{m}}} \Delta C_{\mathrm{p}} \mathrm{d}T \tag{11}$$

and

$$\Delta S = \Delta S_{\mathrm{m}} - \int_{\mathrm{T}}^{T_{\mathrm{m}}} \Delta C_{\mathrm{p}} \frac{\mathrm{d}T}{T} \tag{12}$$

where, ΔS_{m}, ΔH_{m} and T_{m} are the entropy, enthalpy and temperature of fusion, respectively. They are related to each other by the relation: $\Delta S_{\mathrm{m}} = \Delta H_{\mathrm{m}}/T_{\mathrm{m}}$. ΔC_{p} is the difference in specific heats of liquid phase and crystalline phase. In the case of non-availability of ΔC_{p} some approximated theoretical models have been proposed, which result in the different expression of ΔG.

Turnbull [23] assumed ΔC_{p} to be zero. So ΔG can be written as

$$\Delta G = \Delta H_{\mathrm{m}} \left(\frac{\Delta T}{T_{\mathrm{m}}} \right) \tag{13}$$

ΔC_{p} is assumed to be constant under condition of small undercooling. So ΔG can be written as

$$\Delta G = \Delta S_{\mathrm{m}}(T_{\mathrm{m}} - T) + \Delta C_{\mathrm{p}} \left[T \ln \left(\frac{T_{\mathrm{m}}}{T} \right) - (T_{\mathrm{m}} - T) \right] \tag{14}$$

Thompson and Speapen (TS) [17] gave the following expression of ΔG, assuming ΔC_{p} to be constant:

$$\Delta G = \frac{\Delta H_{\mathrm{m}} \Delta T}{T_{\mathrm{m}}} \left(\frac{2T}{(T + T_{\mathrm{m}})} \right) \tag{15}$$

Lad et al. [24] (Lad-1) assumed $\Delta C_{\mathrm{p}} = \Delta H_{\mathrm{m}}/T_{\mathrm{m}}$ and used Taylor series expansion of $\ln(T_{\mathrm{m}}/T) = \ln(1 + \Delta T/T) = \Delta T[1 - \Delta T/2T]/T$, retaining terms up to second order and derived the expression:

$$\Delta G = \frac{\Delta H_{\mathrm{m}} \Delta T}{T_{\mathrm{m}}} \left(1 - \frac{\Delta T}{2T} \right) \tag{16}$$

Again, considering Taylor series expansion of $\ln(T_{\mathrm{m}}/T) = \ln [1 + \Delta T/(T_{\mathrm{m}} + T)/2]$ and retaining up to second-order terms i.e., $\ln(T_{\mathrm{m}}/T) = 4T\Delta T/(T_{\mathrm{m}} + T)^2$ Lad et al. [25] (Lad-2) gave the following expression:

$$\Delta G = \frac{\Delta H_{\mathrm{m}} \Delta T}{T_{\mathrm{m}}} \left(\frac{4T^2}{(T + T_{\mathrm{m}})^2} \right) \tag{17}$$

Another approximation for ΔC_{p} is considering the hyperbolic variation ($\Delta C_{\mathrm{p}} = \Delta C_{\mathrm{p}}^{\mathrm{m}} T_{\mathrm{m}}/T$). Dhurandhar et al. [26] assumed the variation of ΔC_{p} to be inversely varying with temperature.

$$\Delta G = \frac{\Delta H_{\mathrm{m}} \Delta T}{T_{\mathrm{m}}} - \Delta C_{\mathrm{p}}^{\mathrm{m}} T_{\mathrm{m}} \left[\ln \frac{T_{\mathrm{m}}}{T} - \frac{\Delta T}{T_{\mathrm{m}}} \right] \tag{18}$$

Singh and Holz [27] derived an expression for ΔG, assuming a linear variation of ΔC_{p} with T i.e., $\Delta C_{\mathrm{p}} = \mathrm{A}T + \mathrm{B}$, where A and B are unknown constants. Making use of this expression of ΔC_{p} in Eqs. (10)–(12), and using an ansatz, derived the expression of ΔG as:

$$\Delta G = \frac{\Delta H_{\mathrm{m}} \Delta T}{T_{\mathrm{m}}} \left(\frac{7T}{T_{\mathrm{m}} + 6T} \right) \tag{19}$$

Determination of R_{c} from TTT curves

A TTT diagram corresponding to a critical volume fraction of $X = 10^{-6}$ can now be constructed. By substituting the expression of $\eta(T)$ and the different expressions of ΔG i.e., Eq. (13) and from Eq. (15) to (18), the corresponding TTT curves for Pd-based alloys were obtained. So the R_{c} for the glass formation of Pd-based alloys can be given by nose method [8] as:

$$R_{\mathrm{c}} = \frac{T_{\mathrm{m}} - T_{\mathrm{n}}}{t_{\mathrm{n}}} \tag{20}$$

where T_{m} is the melting temperature, T_{n} and t_{n} are the temperature and time corresponding to the nose of TTT curves, respectively.

Results and discussion

Determination of ΔG using different theoretical models

Several Pd-based alloys form BMGs which are known for their good GFA. In the present study, we have investigated the GFA of five different Pd-based alloys. In order to check the applicability of various GFA parameters, they are correlated with R_{c}. So, determination of R_{c} is important for studying the GFA of metallic glasses. The evaluation of R_{c} requires the knowledge of ΔG. A low value of ΔG implies that a larger embryo for nucleation is required, which will require greater chemical fluctuations. Hence, the value of ΔG between liquid and crystal phases will be smaller [28]. Small ΔG also indicates small free volume in a metallic

glass. This enhances the formation of short range order in the alloy near melting point. So, for a good glass-forming system, the values of ΔG and R_c need to be smaller. A smaller value of ΔG indicates smaller nucleation (I_v) and growth rates (u), as indicated by Expressions (2) and (7). Lower I_v and u corresponds to lower crystallization rate, hence greater GFA. Figure 1 shows variation of ΔG with temperature, calculated by different theoretical approaches. The ΔG (T_g) values for different alloy compositions, by different theoretical approaches, are shown in Table 1.

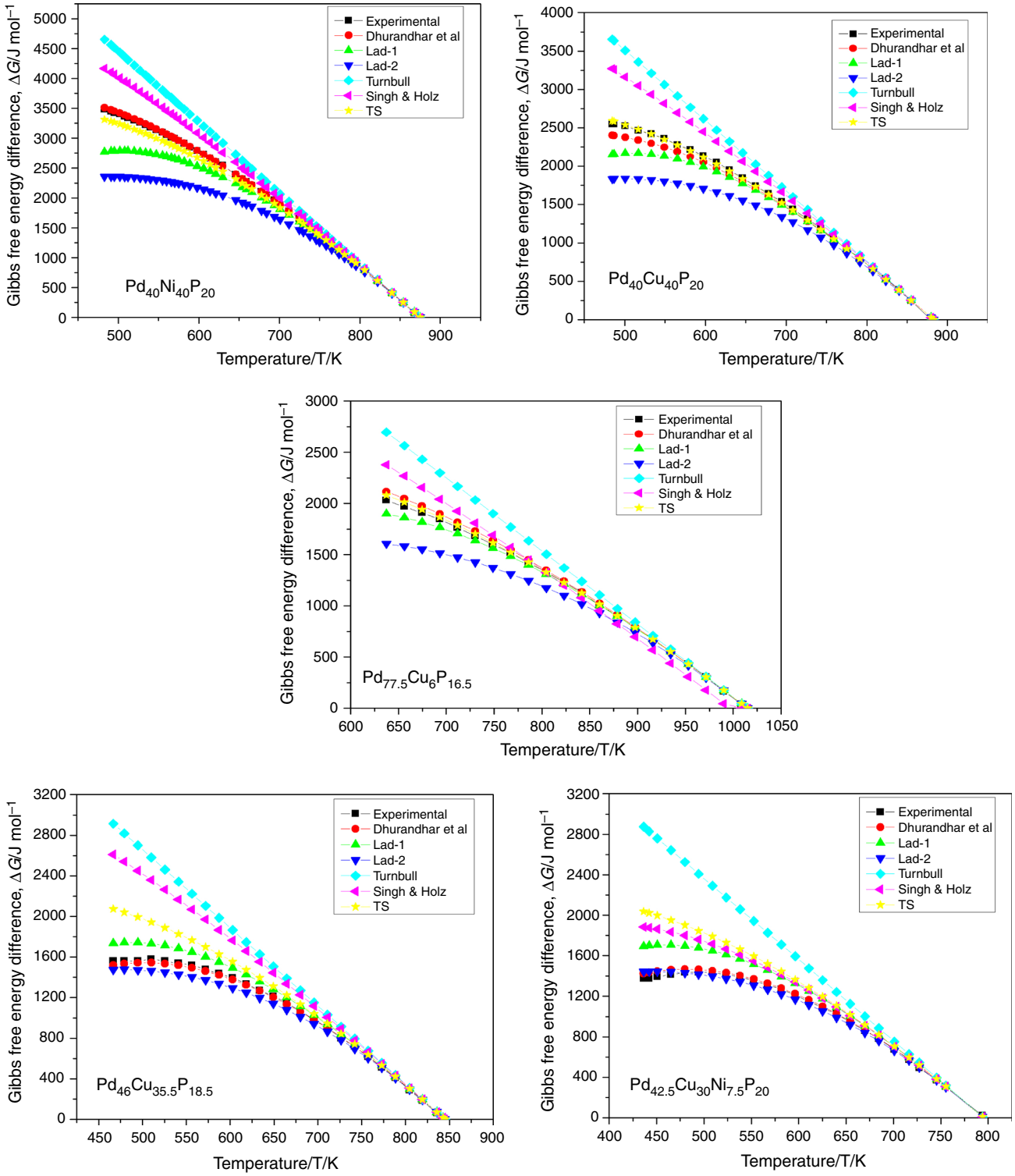

Fig. 1 Variation of ΔG with temperature for Pd-based metallic glasses

Table 1 ΔG (T_g) values for various Pd-based alloys by different methods

Alloys	$\Delta G/T_g$/J mol^{-1}						
	Expt. [12]	Dhurandhar et al. (hyperbolic)	Lad-1	Lad-2	Turnbull	Singh and Holz	TS
$Pd_{40}Ni_{40}P_{20}$	2953.83	2954.84	2631.44	2240.10	3553.83	3308.48	2881.07
$Pd_{40}Cu_{40}P_{20}$	2400.00	2288.41	2152.76	1816.68	3183.12	2913.66	2404.72
$Pd_{77.5}Cu_6Si_{16.5}$	2030.77	2110.51	1895.55	1603.43	2685.71	2695.87	2075.17
$Pd_{46}Cu_{35.5}P_{18.5}$	1497.44	1518.49	1642.46	1399.00	2211.09	2059.74	1758.78
$Pd_{42.5}Cu_{30}Ni_{7.5}P_{20}$	1312.82	1315.75	1442.76	1254.44	1794.82	1699.57	1500.49

In present work, we have calculated ΔG values in entire undercooled region, using different expressions available in literature [17, 23–27]. Various expressions used here are based on different dependence of ΔC_p on temperature. Turnbull expression considers ΔC_p to be equal to zero. In general, ΔC_p is found to decrease with increase in temperature for metallic glasses. Also ΔG does not increase rapidly and shows saturation at large ΔT. Since, Turnbull expression does not involve any variation in ΔC_p with temperature; hence it provides good results in smaller undercooled region, but fails to account for nonlinearity in large undercooled region for metallic glasses. Further, the expressions given by Lad et al. [24, 25] are based on constant ΔC_p approximation, given by $\Delta C_p = \Delta H_m/T_m$. These expressions fairly explain the nonlinearity in ΔG, particularly at large ΔT, for few metallic glass systems and it clearly shows the improvement of the proposed expression given by Eqs. (16) and (17) over Turnbull expression [23]. Also these expressions are widely used for metallic glasses, since they require lesser number of experimental parameters for ΔG calculations. But they fail to explain the variation of ΔG with temperature for a wide range of metallic glasses.

It can be observed from Fig. 1 that for $Pd_{42.5}Cu_{30}Ni_{7.5}P_{20}$ metallic glass, the result obtained by Lad-2 expression lies in close agreement with the experimental values of ΔG, but Lad-1 overestimates the experimental values. For alloys $Pd_{40}Cu_{40}P_{20}$, $Pd_{40}Ni_{40}P_{20}$, and $Pd_{77.5}Cu_6Si_{16.5}$, the expressions given by Lad et al. underestimate the experimental values. Hence, Lad-1 and Lad-2 expressions show different variation for different glassy systems and therefore they are not suitable to study the variation of ΔG for Pd-based metallic glasses. ΔG values were also calculated using expression given by Dhurandhar et al. [26]. The values obtained by this expression perfectly matches with the experimental values in all systems.

Furthermore, we have also used expression given by Singh and Holz Eq. (19), which involves linear variation of ΔC_p with temperature. Moreover, it is derived using an ansatz for explaining the temperature dependence of ΔC_p. The values of ΔG calculated by this expression overestimate the experimental values for all Pd-based alloys. Hence it does not account for the variation of ΔG with T in entire undercooled region. TS expression explains the nonlinearity in the entire undercooled region. It can be seen from Fig. 1 that for $Pd_{40}Cu_{40}P_{20}$ and $Pd_{77.5}Cu_6Si_{16.5}$ metallic glasses, the values of ΔG obtained by TS expression superimposes the experimental values. But for other three systems, it does not give accurate results. Table 1 reports the values of ΔG at T_g.

ΔG (T_g) is a good indicator of the glass-forming ability of metallic glasses. Among various Pd-based alloys, $Pd_{42.5}Cu_{30}Ni_{7.5}P_{20}$ system possesses the lowest value of ΔG (T_g). Hence, it has the highest GFA. This is in accordance with the Inoue's empirical rules [29, 30], which states that the GFA of a metallic glass increases with the increase in the number of alloying elements. Even a minor change in composition of metallic glasses affects the GFA greatly. From above compositions, it can be seen that minor addition of Ni to $Pd_{40}Cu_{40}P_{20}$ alloy increases its GFA by almost twice the value. It can be observed from Table 1 that expression given by Dhurandhar et al. provides value of ΔG (T_g) very close to the experimental values for all the Pd-based alloys. Further, ΔG values calculated by this expression also provide a good match with the experimental results in the entire undercooled region as observed from Fig. 1. Turnbull expression for ΔG was used which gives very crude results in case of BMGs.

The GFA of metallic glasses are supposed to increase as size mismatch among the constituent atoms increase. The atomic radii of Pd, Ni, Cu, Si and P are 140, 149, 145, 110, 98 pm, respectively. It can be observed from the atomic size that for some glasses size mismatch does not effectively reflects the GFA of metallic glass, such as the GFA of $Pd_{40}Ni_{40}P_{20}$ metallic glass is smaller than that of $Pd_{40}Cu_{40}P_{20}$ metallic glass, although the atomic sizes of their components are almost same. So size mismatch can not always justify the GFA of metallic glasses.

Another criterion for glass formation is negative heat of mixing. The mixing enthalpy of stable metallic liquid can be given by [31]:

$$\Delta H^{mix} = 4 \sum_{i=1, i\neq j}^{n} \Delta H_{AB}^{mix} C_i C_j \tag{21}$$

where, ΔH^{mix} is the mixing enthalpy between A and B components, C_i is the atomic percentage of ith component.

The mixing entropy for multicomponent system can be given by following equation [32]:

$$\Delta S^{\text{mix}} = -R \sum_{i=1}^{n} C_i \ln \varphi_i \tag{22}$$

where R is the gas constant, φ_i is the atomic volume fraction of the ith component and can be written as:

$$\varphi_i = \frac{C_i r_i^3}{\sum_{i=1}^{n} C_i r_i^3} \tag{23}$$

where r_i is the atomic radius. The mixing enthalpies and entropies of Pd-based metallic glasses are represented in Table 2.

The mixing enthalpy (ΔH^{mix}) characterizes the chemical interactions between the constituent elements of the metallic glass. If the chemical interactions among the constituent elements of the glass are more, then the long distance diffusion of atoms becomes difficult [33]. Formation of local atomic clusters takes place that results in large negative mixing enthalpy and thereby large GFA. But if ΔH^{mix} values are very large, i.e., the components have a very strong interactions among themselves, it may result in the formation of stable crystal nuclei. Hence, a very large value of ΔH^{mix} may degrade the GFA of metallic glasses. On the other hand, if the chemical interactions are very small, long distance diffusion of atoms will occur easily and formation of new nuclei will take place thereby resulting in formation of new crystal structure. Thus, for the formation of a homogeneous glassy phase with a high GFA, the value of ΔH^{mix} should be moderate. Further, small mixing entropy implies less disordered atomic structures. The diffusion of atoms becomes easier if the metallic glass is less disordered. Consequently, it takes less time for the liquid to form a new ordered structure. Hence, the GFA of metallic glass becomes less. Therefore for good GFA high value of ΔS^{mix} is necessary. In present case, $Pd_{77.5}Cu_6Si_{16.5}$ has the highest value of ΔH^{mix} and the lowest value of ΔS^{mix}, but it is neither the best nor the worst glass former among all the compositions. $Pd_{42.5}Cu_{30}Ni_{7.5}P_{20}$ is found to be the best glass former having moderate value of ΔH^{mix} and highest value of ΔS^{mix}. But, all the other glasses do not strictly follow the above mentioned criteria.

Table 2 Calculated mixing enthalpies and entropies, and critical sizes (Z_c) of Pd-based metallic glasses

Composition	ΔH^{mix}/ kJ mol^{-1}	ΔS^{mix}/ J K^{-1} mol^{-1}	Z_c mm^{-1} [12]
$Pd_{40}Ni_{40}P_{20}$	−22.72	9.56	25
$Pd_{40}Cu_{40}P_{20}$	−26.24	9.48	2
$Pd_{77.5}Cu_6Si_{16.5}$	−31.48	5.79	1
$Pd_{46}Cu_{35.5}P_{18.5}$	−26.15	9.14	12
$Pd_{42.5}Cu_{30}Ni_{7.5}P_{20}$	−25.46	10.97	72

Effect of different models of ΔG in calculation of R_c

Slower cooling rates impose a higher barrier for crystallization. In order to crystallize, the glass-forming melt requires a large amount of energy to overcome the energy barrier. Hence, crystallization becomes difficult at slower cooling rates, which thereby increases the ability of the metallic alloy to form glass. The knowledge of R_c provides an insight it to study the GFA of metallic glasses. Weinberg et al. [34] explained that R_c is sensitive to material parameters which are present in I_v and u expressions. Since the evaluation of I_v and u requires many parameters to be determined, theoretical approximations for various parameters are considered.

Xu et al. [35] fitted the experimental TTT curves for $Pd_{40}Cu_{30}P_{20}Ni_{10}$ and $Zr_{41.2}Ti_{13.8}Cu_{12.5}Ni_{10}Be_{22.5}$ metallic glasses, by varying different parameters in nucleation and growth expression. Then R_c was calculated by continuous integral method in the framework of classical theory. In present work, various expressions of ΔG discussed above are used to calculate I_v and u for Pd-based alloys. Finally,

Table 3 Critical cooling rate (R_c) values for various Pd-based alloys by different methods

Alloys	Critical cooling rate R_c/K s^{-1}						
	Expt [12]	Dhurandhar et al. (hyperbolic)	Lad-1	Lad-2	Turnbull	Singh and Holz	TS
$Pd_{40}Ni_{40}P_{20}$	3.83×10^{-6}	2.1×10^{-6}	4.9×10^{-8}	4.09×10^{-11}	2.53×10^{-4}	4.61×10^{-5}	4.77×10^{-7}
$Pd_{40}Cu_{40}P_{20}$	7.60×10^{-3}	1.23×10^{-3}	5.01×10^{-4}	1.93×10^{-6}	0.346	0.1	2.88×10^{-3}
$Pd_{77.5}Cu_6Si_{16.5}$	1.30	0.9	0.161	1.61×10^{-3}	35.01	11.33	0.60
$Pd_{46}Cu_{35.5}P_{18.5}$	5.95×10^{-5}	1.59×10^{-5}	2.49×10^{-4}	1.63×10^{-6}	0.088	0.026	1.01×10^{-3}
$Pd_{42.5}Cu_{30}Ni_{7.5}P_{20}$	2.51×10^{-8}	1.08×10^{-8}	4.17×10^{-7}	1.38×10^{-9}	6.70×10^{-5}	6.70×10^{-5}	1.65×10^{-6}

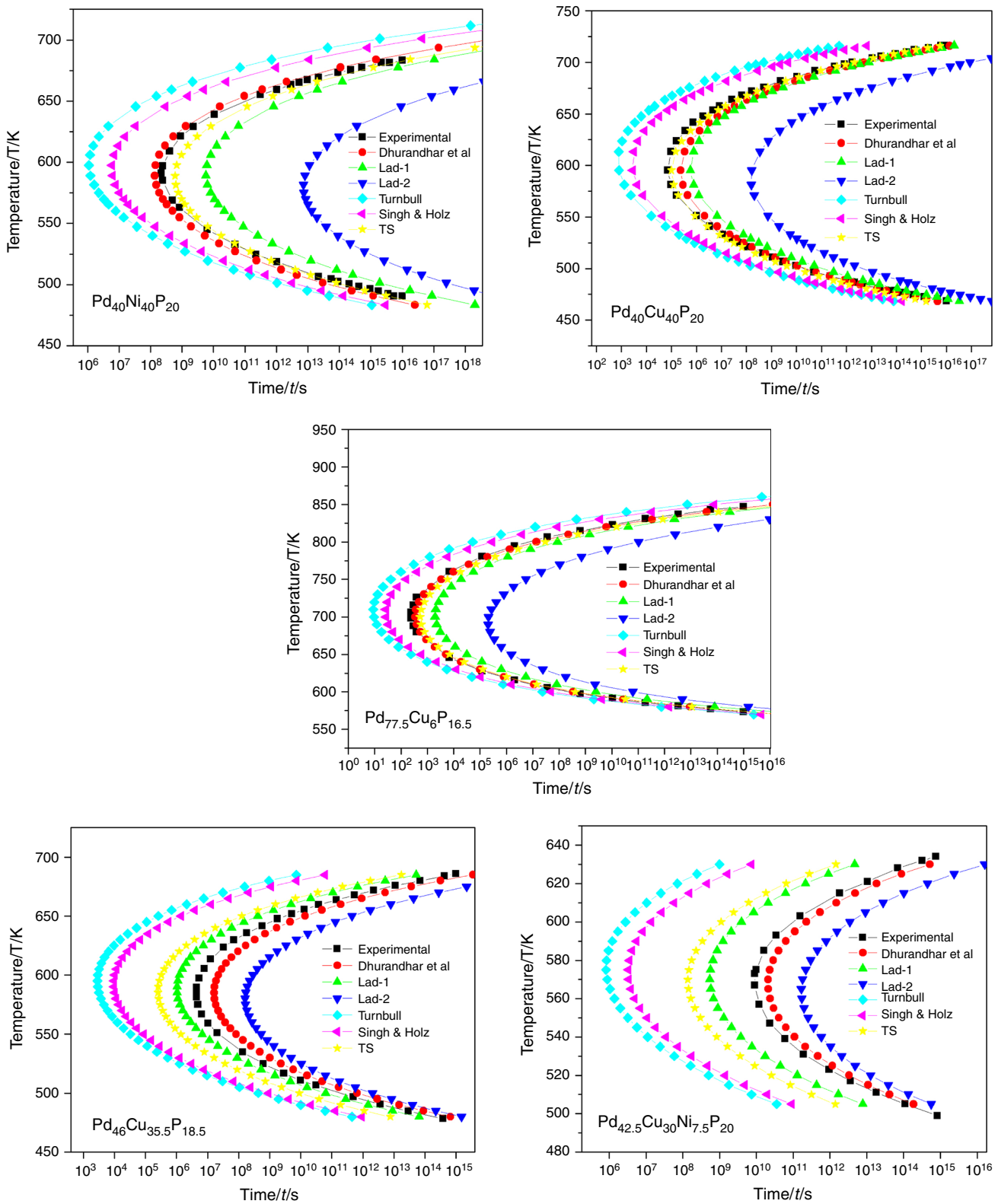

Fig. 2 Calculated TTT curves for Pd-based metallic glasses by different expression of ΔG

TTT curves are constructed using Davis Uhlmann's theory [5] for homogeneous nucleation in the framework of classical nucleation theory.

The R_c values, determined from TTT curves using different expressions of ΔG, are shown in Table 3. It indicates that R_c obtained using different expression of ΔG vary

within few orders of magnitude than the experimental result. The R_c values obtained by Turnbull and Singh and Holz method overestimates the value of R_c calculated by using experimental ΔG, whereas Lad-1 and Lad-2 underestimate the results. The variation in the value of R_c by different model of ΔG may be due to reason that all the expression are derived from different approximation of ΔC_p. However, the result obtained by Dhurandhar et al. expression clearly indicate that it gives better agreement with experimental data in calculating R_c for glass transition of Pd-based alloys. Therefore, this should be appropriate for determining ΔG for Pd-based alloys. So, the variation in ΔG affects the calculation of R_c due to the change in location of maximum crystallization rate. It is observed from Fig. 2, that when the number of components increases from 3 to 4, the C-curve shifts toward right, i.e., the metallic alloy can stay in its supercooled liquid state for a longer time thereby reducing its R_c and increasing GFA. In present case, t_n for $Pd_{46}Cu_{35.5}P_{18.5}$ metallic glass is of the order 10^6 s, whereas for $Pd_{42.5}Cu_{30}Ni_{7.5}P_{20}$ it is of the order 10^9 s. So, an increase in number of components reduces R_c and increases GFA.

Based on high Z_c and low R_c values, the alloys can be arranged in increasing order of GFA as $Pd_{40}Ni_{40}P_{20}$, $Pd_{40}Cu_{40}P_{20}$, $Pd_{77.5}Cu_6Si_{16.5}$, $Pd_{46}Cu_{35.5}P_{18.5}$ and $Pd_{42.5}Cu_{30}Ni_{7.5}P_{20}$. It can be seen from Table 2, that $Pd_{42.5}Cu_{30}Ni_{7.5}P_{20}$ alloy has highest value of Z_c and lowest value of R_c and ΔG. This proves its better GFA over all other metallic glasses. On the other hand, $Pd_{40}Ni_{40}P_{20}$ metallic glass is supposed to have second highest GFA, next to the $Pd_{42.5}Cu_{30}Ni_{7.5}P_{20}$ alloy, based on its second highest Z_c value and smaller R_c value. But ΔG values are not able to reflect the same order of GFA for these metallic glasses.

The value of R_c obtained suggests that calculated results reflect the GFA of Pd-based alloys. The TTT curves of the Pd-based alloy calculated by application of different models of ΔG are shown in Fig. 2. The TTT curves results in "C" shape because of competition between increasing driving force for crystallization and slowing down of kinetics (effective diffusivity) of atom movement [36]. Also during the non-isothermal cooling the major contribution for the total volume crystallized comes from the temperature region in the vicinity of nose [8]. The transformation (liquid-to-crystal) accelerates with an increase in under cooling. The maximum transformation rate is obtained at the nose of the TTT curve. It can be seen that at the nose point cooling rate is high enough to form a glass. Below nose temperature, the driving force for transformation continues to increase but the reaction is now impeded by slow diffusion. Hence, the position of nose in the TTT curve determines the R_c to be used in order to obtain glass. By application of different theoretical expressions of ΔG in nucleation and growth rate equation, it can be observed that the nose of TTT curve is shifted significantly. The decrease in driving force results in decrease in R_c due to shifting of nose toward longer time, which reflects better GFA. So, the calculation of R_c depends on the temperature range under consideration. In small undercooled region the theoretical ΔG values lies close to experimental values, so if R_c is calculated in this region, the choice of expression for ΔG will not make any significant difference in results.

Conclusions

The R_c values for the glass formation of Pd-based metallic glasses have been estimated by TTT calculations. Different models of ΔG were incorporated in nucleation and growth rate expression to evaluate R_c. The result obtained by expression given by Dhurandhar et al. (hyperbolic) for ΔG gives the best estimation for R_c for the glass formation of Pd-based alloys. The driving force of crystallization affects the estimation of R_c in large undercooled region, but in lower undercooling it does not make a significant difference. The present study suggests that the thermodynamic quantity ΔG of the under cooled liquid is indispensible for estimation of TTT curves. $Pd_{42.5}Cu_{30}Ni_{7.5}P_{20}$ metallic glass is found to be the best glass former among all Pd-based metallic glasses.

Acknowledgements One of the authors (Sonal Prajapati) is grateful to Department of Science and Technology (DST), Govt. of India, for providing financial assistance under the DST-INSPIRE fellowship scheme. Supriya Kasyap is grateful to the University Grant Commission (UGC), New Delhi for providing the financial support under Research Fellowship in Science for Meritorious Students (RFSMS) scheme.

References

1. Singh PK, Dubey KS. Analysis of thermodynamic behaviour of bulk metallic glass forming melts and glass forming ability. J Therm Anal Calorim. 2010;100:347–53.
2. Wu J, Pan Y, Huang J, Pi J. Non-isothermal crystallization kinetics and glass forming ability of Cu–Zr–Ti–In bulk metallic glasses. Thermochim Acta. 2013;552:15–22.
3. Schawe JEK. The Gibbs free energy difference between a supercooled melt and the crystalline phase of polymers. J Therm Anal Calorim. 2015;120:1417–25.
4. Patel AT, Shevde HR, Pratap A. Thermodynamics of $Zr_{52.5}Cu_{17.9}Ni_{14.6}Al_{10}Ti_5$ bulk metallic glass forming alloy. J Therm Anal Calorim. 2012;107:167–70.
5. Uhlmann DR. A kinetic treatment of glass formation. J Non Cryst Solids. 1972;7:337–48.
6. Rodova M, Liska M, Nitsch K, Kozisek Z. Solidification of molten zinc chloride experimental and theoretical studies. J Therm Anal Calorim. 2008;91:181–5.
7. Schroers J, Wu Y, Busch R, Johnson WL. Transition from nucleation controlled to growth controlled crystallization in $Pd_{43}Ni_{10}Cu_{27}P_{20}$ melts. Acta Mater. 2001;49:2773–81.
8. Weinberg MC, Uhlmann DR. "Nose method" of calculating critical cooling rates for glass formation. J Am Ceram Soc. 1989;72:2054–8.

9. Uhlmann DR, Klein L, Onorato PIK, Hopper RW. The formation of lunar breccias: sintering and crystallization kinetics. In: Proceedings lunar science conference 6th; 1975. p. 693–705.
10. Inoue A. Stabilization of metallic supercooled liquid and bulk amorphous alloys. Acta Mater. 2000;48:279–306.
11. Nishiyama N, Inoue A. Direct comparison between critical cooling rate and some quantitative parameters for evaluation of glass-forming ability in Pd–Cu–Ni–P alloys. Mater Trans. 2002;43(8):1913–7.
12. Haruyama O, Watanabe T, Yuki K, Horiuchi M, Kato H, Nishiyama N. Thermodynamic approach to glass-forming ability of water-quenched Pd–P-based and $Pt_{60}Ni_{15}P_{25}$ bulk metallic glasses. Phys Rev B. 2011;83:064201.
13. Nishiyama N, Inoue A. Flux treated Pd–Cu–Ni–P amorphous alloy having low critical cooling rate. Mater Trans JIM. 1997;38(5):464–72.
14. Xu D, Wirth BD, Schroers J, Johnson WL. Calculating glass-forming ability in absence of key kinetic and thermodynamic parameters. Appl Phys Lett. 2010;97:024102.
15. Kim JH, Park JS, Park ES, Kim WT, Kim DH. Estimation of critical cooling rates for glass formation in bulk metallic glasses through non-isothermal thermal analysis. Met Mater Int. 2005;11(1):1–9.
16. Xu K, Wang Y, Li J, Li Q. Critical cooling rate for the glass formation of ferromagnetic $Fe_{80}P_{13}C_7$ alloy. Acta Metall Sin. 2013;26(1):56–62.
17. Thompson CV, Spaepen F. On the approximation of the free energy change on crystallization. Acta Metall. 1979;27:1855–9.
18. Ge L, Hui X, Chen G, Liu Z. Prediction of the glass-forming ability of Cu–Zr binary alloys. Acta Phys Chim Sin. 2007;23(6):895–9.
19. Nishiyama N, Inoue A. Supercooling investigation and critical cooling rate for glass formation in Pd–Cu–Ni–P alloy. Acta Mater. 1999;47(5):1487–95.
20. Herlach D. Non-equilibrium solidification of undercooled melts. Mater Sci Eng R. 1994;12:177–272.
21. Miller WA, Chadwick GA. On the magnitude of the solid/liquid interfacial energy of pure metals and its relation to grain boundary melting. Acta Metall. 1967;15(4):607–14.
22. Kittel C. Introduction to solid state physics. New York: Wiley; 2005 **71**.
23. Turnbull D. Under what conditions can a glass be formed? Contem Phys. 1969;10(5):473–88.
24. Lad KN, Pratap A, Raval KG. Estimation of the free energy change on crystallization of multicomponent glass forming alloys. J Mater Sci Lett. 2002;21:1419–22.
25. Lad KN, Raval KG, Pratap A. Estimation of Gibbs free energy difference in bulk metallic glass forming alloys. J Non Cryst Solids. 2004;334–335:259–62.
26. Dhurandhar H, Rao TLS, Lad KN, Pratap A. Gibbs free energy for the crystallization of metallic glass-forming alloys from an undercooled liquid. Philos Mag Lett. 2008;88(4):239–49.
27. Singh HB, Holz A. Stability limit of supercooled liquids. Solid State Commun. 1983;45(11):985–8.
28. Guo F, Poon S, Shiflet G. Metallic glass ingots based on yttrium. Appl Phys Lett. 2003;83(13):2575–7.
29. Inoue A, Takeuchi A, Zhang T. Ferromagnetic bulk amorphous alloys. Metall Mater Trans A. 1998;29:1779–93.
30. Inoue A. High strength bulk amorphous alloys with low critical cooling rates. Mater Trans JIM. 1995;36:866–75.
31. Xia M, Zhang S, Li J, Ma C. Thermal stability and its prediction of bulk metallic glass systems. Appl Phys Lett. 2006;88:261913.
32. Jiang Q, Chi BQ, Li JC. A valence electron concentration criterion for glass-formation ability of metallic liquids. Appl Phys Lett. 2003;82:2984.
33. Wang D, Huang Y, Shen J. Thermodynamic characteristics of Ti-based glass-forming alloys. J Non Cryst Solids. 2009;355:986–90.
34. Weinberg MC, Zelinski BJ, Ulhmann DR. Critical cooling rate calculations for glass formation. J Non Cryst Solids. 1990;123:90–6.
35. Xu D, Johnson WL. Crystallization kinetics and glass-forming ability of bulk metallic glasses $Pd_{40}Cu_{30}Ni_{10}P_{20}$ and $Zr_{41.2}Ti_{13.8}Cu_{12.5}Ni_{10}Be_{22.5}$ from classical theory. Phys Rev B. 2006;74:024207.
36. Uhlmann DR. Glass formation. J Non Cryst Solids. 1977;25:42–85.